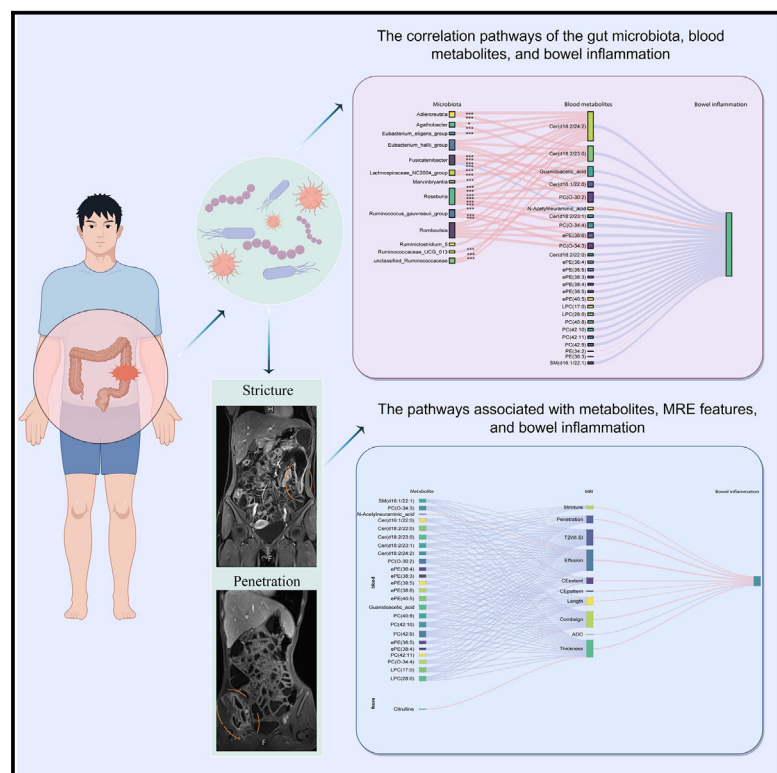


Altered gut microbiome-metabolite interactions link intestinal inflammation severity and MR enterography abnormalities in Crohn's disease

Graphical abstract



Authors

Ruonan Zhang, Zhoulei Li, Li Huang, ..., Shaochun Lin, Yejun Wang, Xuehua Li

Correspondence

lshchun@mail.sysu.edu.cn (S.L.),
wangyj@szu.edu.cn (Y.W.),
lxueh@mail.sysu.edu.cn (X.L.)

In brief

Microbiology; Bioinformatics; Omics

Highlights

- The research integrates gut microbes–metabolite interactions with MRE features
- Multi-metabolites regulate bowel inflammation resulting in morphological alterations
- Serum N-acetylneuraminic and guanidinoacetic acid relate to inflammatory MRE features
- *Ruminococcus gnavreaii* inhibits inflammation by regulating specific metabolites



Article

Altered gut microbiome-metabolite interactions link intestinal inflammation severity and MR enterography abnormalities in Crohn's disease

Ruonan Zhang,^{1,5} Zhoulei Li,^{1,5} Li Huang,^{1,5} Weimiao Kong,^{2,3} Yidong Zheng,^{2,3} Yangdi Wang,¹ Xiaodi Shen,¹ Lili Huang,¹ Xinyue Wang,¹ Qingzhu Zheng,¹ Luyao Wu,¹ Yaoqi Ke,¹ Ren Mao,⁴ Zhenpeng Peng,¹ Canhui Sun,¹ Shi-Ting Feng,¹ Shaochun Lin,^{1,*} Yejun Wang,^{4,*} and Xuehua Li^{1,6,*}

¹Department of Radiology, The First Affiliated Hospital of Sun Yat-Sen University, 58 Zhongshan II Road, Guangzhou 510080, People's Republic of China

²Youth Innovation Team of Medical Bioinformatics, Shenzhen University Medical School, Shenzhen 518060, China

³Department of Cell Biology and Genetics, College of Basic Medicine, Shenzhen University Medical School, Shenzhen 518060, China

⁴Department of Gastroenterology, The First Affiliated Hospital of Sun Yat-Sen University, 58 Zhongshan II Road, Guangzhou 510080, P.R. China

⁵These authors contributed equally

⁶Lead contact

*Correspondence: lschun@mail.sysu.edu.cn (S.L.), wangyj@szu.edu.cn (Y.W.), lxueh@mail.sysu.edu.cn (X.L.)

<https://doi.org/10.1016/j.isci.2025.112310>

SUMMARY

Altered gut microbiota–metabolite interactions may result in intestinal inflammation severity variation in Crohn's disease (CD). Magnetic resonance enterography (MRE) advances anti-inflammatory strategy development. We aimed to identify inflammation-related multiomics factors and MRE interactions for CD management, analyzing 425 CD patients and 42 healthy controls undergoing MRE, ileocolonoscopy, and fecal/blood sampling (microbiota/metabolite analyses), with intestinal inflammation categorized by MRE and ileocolonoscopy. *Ruminococcus* species were enriched in CD patients versus healthy controls, while *Pseudomonas* and *Staphylococcus* dominated moderate–severe versus no–mild inflammation groups, suggesting inflammation-level associations. *Ruminococcus gausvreaui* suppressed intestinal inflammation by regulating serum PC(O-34:3), ePE(38:6), and ceramides (all $p < 0.05$). Serum N-acetylneuraminic acid and guanidinoacetic acid correlated with intestinal morphological changes (e.g., MRE-detectable effusion and wall thickness) and inflammation severity ($P_{ACME} < 0.05$). A link was established between microscopic microbiota-metabolite markers and macroscopic imaging of inflammatory features, which could offer valuable insights into inflammation management.

INTRODUCTION

Inflammatory bowel diseases (IBDs), including Crohn's disease (CD), affect 6.8 million individuals globally.¹ Significant alterations in the microecological environment of IBD are characterized by an increasing abundance of *Escherichia coli* and decreased levels of short-chain fatty acids.^{2,3} Despite its prevalence CD is currently incurable. Although the use of biologics has reduced the risk of surgery in patients with CD,⁴ some patients still require surgical intervention⁵ due to refractory penetrating and stricturing complications.⁶ Since the risk of postoperative recurrence remains high, patients' microbiome compositions were recognized as key players in this condition.⁷ Multiple surgical resections may lead to short bowel syndrome, further impacting patients' quality of life. Therefore, exploring potential biomarkers related to severe intestinal inflammation is urgently needed to avoid intestinal resection.

Intestinal inflammation in CD patients can be influenced by dysfunctional gut microbiota and metabolites.^{8–11} The investiga-

tion of perturbations in the microbial–metabolome interface may reveal novel therapeutic targets.¹² However, previous studies have focused primarily on conducting comparative analyses between CD and ulcerative colitis.^{13,14} Whether disturbances in the gut microbiota–metabolite interaction can lead to inflammation exacerbation in CD patients remains unclear. Furthermore, the common standards used to assess CD activity rely primarily on laboratory indicators (e.g., fecal calprotectin) or clinical scoring systems (e.g., the Harvey–Bradshaw Index).^{11,15} However, these methods often lack specificity.

Endoscopy and cross-sectional imaging such as magnetic resonance enterography (MRE) are main standards to assess disease activity in CD patients.^{16,17} Gastrointestinal endoscopy is important in the management of CD.¹⁸ The simplified endoscopy for CD (SES-CD) is a reliable scoring system for CD inflammation.¹⁹ MRE is currently the most promising cross-sectional tool for assessing transmural inflammation with high specificity.²⁰ The inclusion of MRE as a standard will increase the precision of evaluating intestinal inflammation. More importantly,



MRE has emerged as a pivotal imaging modality for surgeons to assess inflammatory lesions before surgery, owing to its ability to depict intestinal morphological alterations such as strictures and penetration induced by inflammation.²¹ Therefore, linking the gut microbiota and metabolites to MRE-detected macromorphological changes is highly important for identifying more specific biomarkers related to severe intestinal inflammation or potential surgical outcomes.

In this prospective study involving 467 participants (Table 1), we aimed to investigate the differences in the gut microbiota and fecal and blood metabolites among healthy controls (HCs), CD patients with no–mild bowel inflammation (BI0), and those with moderate–severe bowel inflammation (BI1) to explore novel biomarkers that can potentially inhibit the severe intestinal inflammation. To increase the specificity and clinical translational potential of the identified biomarkers, a combination of MRE and endoscopy was employed for the joint evaluation of intestinal inflammation, and microscopic multiomics factors were linked to MRE-detectable macroscopic morphology through correlation analysis. This unique study design may provide novel insights into the underlying mechanism of intestinal inflammation development and identify possible biomarkers for improving treatment in CD patients.

RESULTS

Alterations in fecal and blood metabolites among HC, BI0, and BI1

Clustering analysis of the fecal and blood metabolites revealed a clear separation between the groups. The HC, BI0, and BI1 groups were significantly separated from each other by fecal metabolites (PERMANOVA test, $p = 0.001$; Figures 1A and 1B) and blood metabolites ($p = 0.001$; Figures 1C and 1D). A visible difference in blood metabolites between the BI0 and BI1 groups was detected, although the difference did not reach statistical significance ($p = 0.151$). These results indicate a metabolite shift during the inflammatory process.

We performed pairwise comparisons and KEGG enrichment analysis to further identify valuable metabolites during inflammation development. In the fecal metabolism analysis, 106 overlapping metabolites were obtained from pairwise comparisons on HC vs. BI0 and HC vs. BI1 (Mann–Whitney U test, $FDR < 0.05$) (Figure 1E). The pathways associated with arginine and proline metabolism, aminoacyl-tRNA biosynthesis, etc., were enriched, with significant differences between HC vs. BI0 and HC vs. BI1. Although no metabolite showed a statistically significant difference between BI0 vs. BI1 (Figure 1E), KEGG analysis revealed a fecal metabolic pathway related to ‘glycine, serine, and threonine metabolism’, which showed enrichment, though lowly significant ($p = 0.047$), in HC vs. BI1, but not in HC vs. BI0 (Figure 1F).

Encouragingly, blood metabolite analysis revealed 26 overlapping metabolites with significant differences in abundance across all three groups (Figure 1G), highlighting the consistent involvement of the ether lipid metabolism pathway (Figure 1H) and suggesting its potential contribution to varying levels of intestinal inflammation. We further examined the expression levels of these 26 overlapping blood metabolites. Among them,

23 metabolites, including guanidinoacetic acid, decreased gradually with increasing inflammatory severity, while N-acetylneuraminic acid was positively correlated with inflammation severity (Figures 2A and 2B). The levels of PE (36:3) and PE (34:2) from HC to BI0 to BI1 initially decreased but then subsequently increased; however, their BI1 levels remained lower than those in HCs. Logistic regression (LR) prediction models were built using these 26 metabolites to differentiate HC from BI0 and BI0 from BI1, achieving satisfactory performance, with roc AUCs of 0.83 and 0.68 (Figure 2C), as assessed with an independent validation dataset.

Collectively, the metabolites significantly differed across the three groups. Among them, guanidinoacetic acid and N-acetylneuraminic acid were detected in both the fecal and blood samples. We further confirmed consistent concentration trends of N-acetylneuraminic acid in both the discovery dataset and the validation dataset with blood and fecal samples; the observed trend was positively correlated with inflammation levels. However, no such trend was observed for guanidinoacetic acid (Figure 2D).

Metabolites as significant biomarkers of intestinal inflammation severity

A machine-learning approach was employed to identify more robust metabolites for inflammation severity. LR was used to identify fecal and blood metabolites significantly contributing to inflammatory classification (Method S1). Between HC vs. BI0, BI0 vs. BI1, and HC vs. BI1, we identified 26, 9, and 24 fecal metabolites, respectively. N-acetylneuraminic acid and guanidinoacetic acid were consistently present in the lists (Figure 3A). Using these fecal metabolites as features, three LR models were trained. The rocAUC reached 0.90, 0.57, and 0.87, respectively, using a validation dataset (Figure 3A). Moreover, 13, 9, and 14 blood metabolites were identified (Figure 3B) and constructed into three better LR models, with a rocAUC of 0.97 for distinguishing BI1 from HC using a validation dataset.

To further improve distinguishing performance, fecal and blood metabolites were integrated to develop composite models, with 17, 19, and 20 of the most significant biomarkers, respectively (Figure 3C). These composite models exhibited superior performance compared with the individual models, with improved cross-validated rocAUC values of 0.99, 0.72, and 1.00 for each respective group. The performance also demonstrated remarkable stability, with rocAUC values of 0.88, 0.67, and 0.99 when applied to the validated dataset (Figure 3C).

Consequently, combining fecal and blood metabolites enhances the prediction of inflammation severity, offering a panel of significant metabolites.

Bacterial species as significant biomarkers of intestinal inflammation severity

We further investigated the differential distribution of bacteria during inflammation stages via fecal 16S rRNA amplicon sequencing. The alpha diversity decreased gradually among the HC, BI0 and BI1 groups (Figure 4A). Analysis of beta diversity with nonmetric multidimensional scaling (NMDS) revealed that intestinal flora characteristics exhibited significant

Table 1. Clinical characteristics of healthy controls and patients with CD

Characteristics	Healthy controls	Discovery dataset				Validation dataset			
		Total	BI0	BI1	<i>P</i> ^b	Total	BI0	BI1	<i>P</i> ^b
Gender, n (%)	<i>n</i> = 42	<i>n</i> = 230	<i>n</i> = 108	<i>n</i> = 122	0.429	<i>n</i> = 195	<i>n</i> = 95	<i>n</i> = 100	0.211
Male	35(83.33%)	184(80%)	84(77.78%)	100(81.97%)		144(73.85%)	74(77.89%)	70(70%)	
Female	7(16.67%)	46(20%)	24(22.22%)	22(18.03%)		51(26.15%)	21(22.11%)	30(30%)	
Age, mean ± SD	29.50 ± 6.19	30.30 ± 7.99	29.82 ± 8.02	30.72 ± 7.98	0.397	28.95 ± 7.20	29.95 ± 7.13	28.01 ± 7.18	0.060
Disease course, month, mean ± SD	N/A	60.26 ± 51.40	66.87 ± 50.67	54.41 ± 51.54	0.066	56.44 ± 49.57	60.44 ± 48.13	52.64 ± 50.85	0.273
Drug use ^a , n (%)	N/A								
Biologics		63(27.39%)	28(25.93%)	35(28.69%)	0.520	85(43.59%)	53(55.79%)	32(32%)	0.001
Corticosteroids		12(5.21%)	4(3.70%)	8(6.56%)	0.606	10(5.13)	4(4.21%)	6(6%)	0.572
Immunomodulator		69(30%)	46(42.59%)	23(18.85%)	0.000	35(17.95%)	24(25.26%)	11(11%)	0.010
5-Aminosalicylic acid		36(15.65%)	15(13.89%)	21(17.21%)	0.528	47(24.10%)	17(17.89%)	30(30%)	0.049
Surgery, n (%)	N/A				0.861				0.209
Intestinal surgery		59(25.65%)	32(29.63%)	27(22.13%)		38(19.49%)	28(29.47%)	10(10%)	
Perianal surgery		35(15.22%)	13(12.04%)	22(18.03%)		19(9.74%)	6(6.32%)	13(13%)	
Montreal classification, n (%)	N/A								
Age					0.285				0.050
A1 [≤16]		2(0.87%)	0	2(1.64%)		0	0	0	
A2 [17–40]		204(88.70%)	98(90.74%)	106(86.89%)		183(93.85%)	88(92.63%)	95(95%)	
A3 [>40]		24(10.43%)	11(10.19%)	13(10.66%)		12(6.15%)	7(7.37%)	5(5%)	
Disease location					0.308				0.091
L1 [terminal ileum]		26(11.30%)	10(9.26%)	16(13.11%)		41(21.03%)	25(26.32%)	16(16%)	
L2 [colon]		9(3.91%)	6(5.56%)	3(2.46%)		8(4.10%)	4(4.21%)	4(4%)	
L3 [ileocolon]		186(80.87%)	85(78.70%)	101(82.79%)		144(73.85%)	65(68.42%)	79(79%)	
L4 [upper gastrointestinal]		9(3.91%)	7(6.48%)	2(1.64%)		2(1.03%)	1(1.05%)	1(1%)	
Disease behavior					0.162				0.209
B1 [inflammatory]		89(38.70%)	44(40.74%)	45(36.89%)		65(33.33%)	38(40.00%)	27(27%)	
B2 [stricturing]		70(30.43%)	44(40.74%)	26(21.31%)		83(42.56%)	34(35.79%)	49(49%)	
B3 [penetrating]		71(30.87%)	20(18.52%)	51(41.80%)		47(24.10%)	23(24.21%)	24(24%)	
Perianal diseases, n (%)	N/A				0.272				0.081
Fistula		115(50%)	51(47.22%)	64(52.46%)		85(43.59%)	41(43.16%)	44(44%)	
Abscess		28(12.17%)	12(11.11%)	16(13.11%)		23(11.79%)	7(7.37%)	16(16%)	
Resection length of bowel (cm)	N/A								
Resection length of small intestine		54.56 ± 41.12	41.64 ± 29.82	70.26 ± 43.20	0.064	43.71 ± 33.71	41.08 ± 23.14	45.00 ± 35.74	0.189
Resection length of colon		8.00[0, 22.00]	4.50[0.00, 4.00]	10.00[0, 22.00]	0.644	10.00[3.75, 21.63]	9.50[0, 10.75]	11[4, 23]	0.219
Smoking, n (%)	5(11.90%)	21(9.13%)	6(5.56%)	15(12.30%)	0.077	7(3.59%)	3(3.16%)	4(4%)	0.753
Drinking, n (%)	21(50%)	16(6.96%)	7(6.48%)	9(7.38%)	0.790	6(3.08%)	5(5.26%)	1(1%)	0.086

(Continued on next page)

Table 1. Continued

Characteristics	Discovery dataset			Validation dataset		
	Healthy controls	Total	P^b	Total	BI0	BI1
BMI, kg/m ² , mean \pm SD	22.93 \pm 2.12	19.96 \pm 3.32	20.34 \pm 3.22	19.62 \pm 3.38	0.103	20.03 \pm 2.97
CRP (mg/L, median [IQR])	N/A	7.03 [1.18, 7.38]	2.53 [0.78, 9.33]	16.10 [3.70, 37.83]	0.000	3.66 [0.92, 19.50]
ESR (mm/h, mean \pm SD)	N/A	30.34 \pm 26.49	14.00 [5.25, 0.50]	34 [15.75, 57.00]	0.000	22.00 \pm 19.98
HB (g/L, mean \pm SD)	N/A	123 \pm 21.76	127.69 \pm 18.86	118.81 \pm 23.34	0.002	122 \pm 22.45
ALB (g/L, mean \pm SD)	N/A	37.30 \pm 6.63	39.36 \pm 7.24	35.47 \pm 5.45	0.000	37.59 \pm 5.35

CD, Crohn's disease; BI0, No-mild bowel inflammation; BI1, Moderate-severe bowel inflammation; BMI, Body mass index; IQR, interquartile range; SD, Standard deviation; ESR, erythrocyte sedimentation rate; CRP, C-reactive protein; HB, Hemoglobin; ALB, albumin; N/A, not applicable.

^aMedicine use within 3 months before inclusion.

^bComparison between no-mild bowel inflammation (BI0) and moderate-severe bowel inflammation (BI1).

discriminatory power among the HC, BI0, and BI1 groups (PERMANOVA test, $p = 0.001$) (Figure 4B). Among them, HCs and BI0/BI1 differentiated significantly from each other; along the different dimensions of NMDS, BI0 and BI1 showed small but not significant difference from each other (Figure 4B).

Similarly, we also conducted a comparative analysis of bacterial composition among groups with different inflammatory levels. Significant differences in intestinal bacterial composition were observed between HCs vs. BI0 and HCs vs. BI1, with 103 and 130 gut microbiota (Mann-Whitney U tests, $FDR < 0.05$), respectively, under an overlap of 97 common gut microbiota (Figure 4C). However, no bacterial composition significantly differed between BI0 and BI1. With a different comparison strategy, LefSe analysis also revealed significant differences between HC vs. BI0 and HC vs. BI1 (84 and 229 gut microbiota, respectively, absolute value of LDA score ≥ 2) (representative results are shown in Figure 4D; complete results are presented in Figures S2 and S3). Notably, there was a high degree of concordance regarding the differential gut microbiota identified by both of the above showed comparisons (Figures S2 and S3). LefSe analysis revealed that the gut microbiota differed between BI0 and BI1: *Pseudomonas* and *Staphylococcus* were more abundant in BI1, whereas *Hafnia-Obesumbacterium* was more abundant in BI0 (Figure 4D). *Pseudomonas* is proinflammatory,²² with 50% of CD patients developing serum antibodies against it.²³ Similarly, *Staphylococcus* stimulates proinflammatory gene expression and cytokine production.²⁴ Moreover, this study may be the first to report a correlation between *Hafnia-Obesumbacterium* and CD-related inflammation, but further investigations are needed to understand its role in reducing the severity of inflammation. For HCs vs. BI0 and HCs vs. BI1, LefSe analyses also revealed many taxa associated with inflammation, including well-known CD-associated species such as *Enterococcus*, *Ruminococcus*, and *Lachnospiraceae* (Figures 4D, S2, and S3). Interestingly, multiple *Ruminococcus* species had different effects.

Again, the taxonomic characteristics that could classify inflammation levels most effectively were analyzed via LASSO, which generated 29 and 21 features between HCs vs. BI0 and HCs vs. BI1, respectively. The LR models exhibited good discrimination for both the training and validation datasets, with rocAUC values of 0.95 and 0.85 for HCs vs. BI0 and 0.85 and 0.94 for HCs vs. BI1, respectively (Figure 4E). However, the model based only on the three gut microbiota types failed to distinguish BI0 and BI1 effectively. It was noted that applying LASSO also identified different species or groups of *Ruminococcus*, a genus closely associated with IBD, including *Ruminococcus gnavus* and *R. gnavreaii*.

Taken together, although the differential flora observed among BI0 vs. BI1 did not exhibit significant discriminative efficacy, we identified several bacteria that may play crucial roles in intestinal inflammation severity variation.

Combining the gut microbiota with fecal and blood metabolites improves the accuracy of characterizing intestinal inflammation severity

The aforementioned results prompted us to investigate whether integrating these multiomics factors can further enhance the

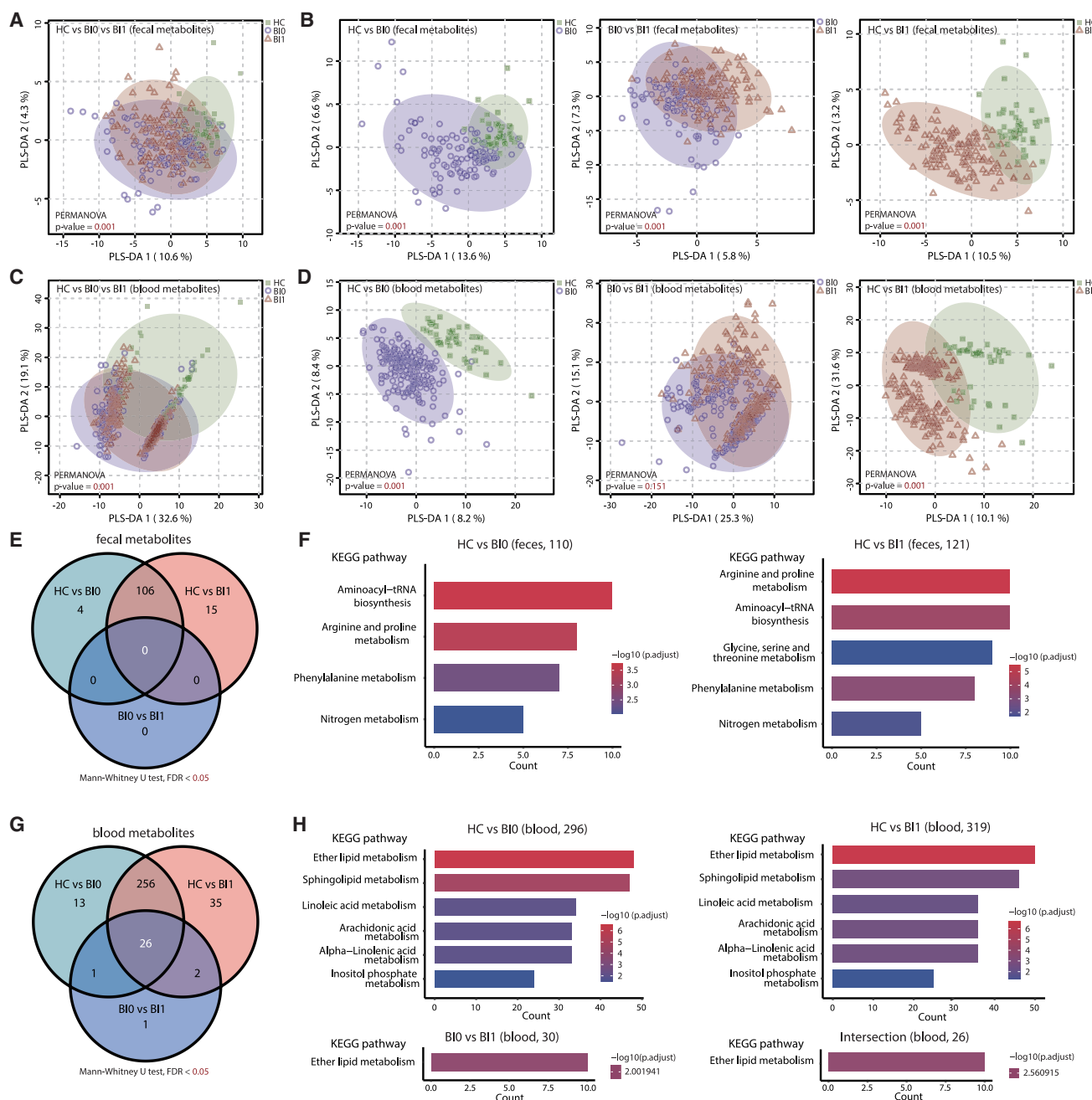


Figure 1. Fecal and blood metabolome comparisons between HCs, BI0, and BI1 patients

(A–D) Clustering of the subjects with fecal (A and B) or blood (C and D) metabolites after PLS-DA analysis. PERMANOVA tests were performed, and the *p* values are indicated.

(E) Comparison of the fecal metabolites between the HC, BI0, and BI1 groups.

(F) Functional enrichment analysis of the significantly different fecal metabolites between the groups is shown.

(G) Comparison of the blood metabolites between the HC, BI0, and BI1 groups.

(H) Functional enrichment analysis of the significant differences in blood metabolites between the groups is shown.

performance in characterizing inflammation severity. Initially, 17, 19, and 20 characteristic metabolite–flora combinations were identified to distinguish HCs vs. BI0, BI0 vs. BI1, and HCs vs. BI1 groups from LASSO regression, respectively (Figures 4F–

4H). The application of these features to train LR models in independent validation datasets yielded satisfactory results in distinguishing HCs vs. BI0 and HCs vs. BI1, with rocAUC values of 0.89 and 0.99, respectively (Figures 4F and 4H). Notably, the BI0

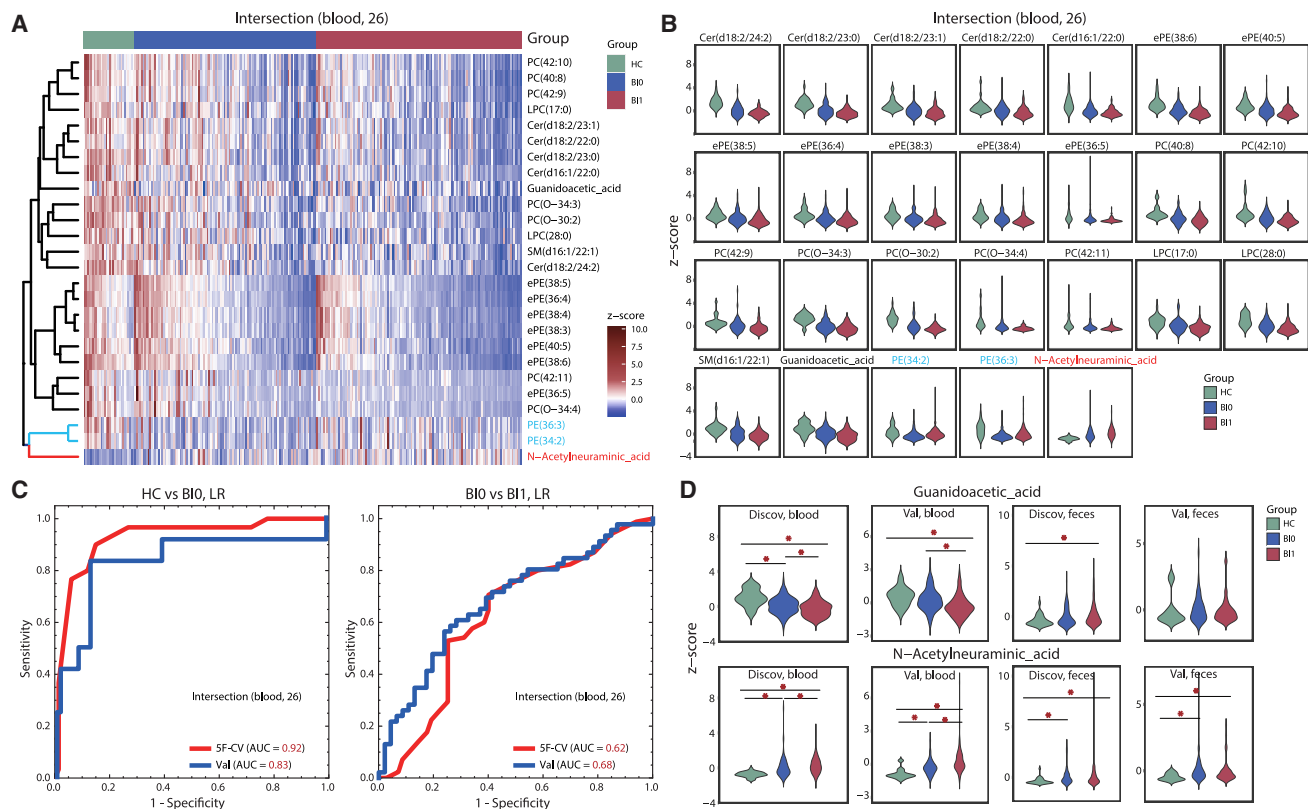


Figure 2. The abundance patterns of 26 blood metabolites were significantly different between each pair of bowel inflammation groups

(A) Abundance heatmap of the 26 blood metabolites.

(B) Violin diagrams showing the abundances of the 26 blood metabolites. All the metabolites are significantly different between each pair of groups ($p < 0.05$, Mann-Whitney U test).

(C) ROC curves of the bowel inflammation prediction models based on the 26 blood metabolites. The average 5-fold cross-validation (5F-CV) curve with the discovery dataset and the independent validation (Val) curve with the validation dataset are shown in red and blue, respectively. The rocAUC was indicated for each model, while for 5F-CV evaluation, the mean of 5-fold rocAUC values was indicated.

(D) Abundances of guanidoacetic acid and N-acetylneuraminic acid in the blood and feces of the discovery and validation datasets. The z-scores of the metabolites for each group in (B) and (D) were represented as mean \pm SEM among the pooled cases. *, $p < 0.05$, Mann-Whitney U test.

vs. BI1 model, which is based on multiomics features, had a rocAUC value of 0.69 for independent assessment with the validation dataset, outperforming the models developed with single omics (Figure 4G).

Accordingly, the combination of metabolites with the gut microbiota enables a more accurate prediction of intestinal inflammation levels.

Interactions between metabolites and the gut microbiota are altered during different intestinal inflammation severity

To elucidate the underlying mechanism of the gut microbiota and metabolites in intestinal inflammation severity, we analyzed possible pathway associations among the gut microbiota, metabolites, and intestinal inflammation. For blood metabolites, we focused on the 26 metabolites that consistently showed significant differences between each pair of intestinal inflammation groups. For the gut microbiota and fecal metabolites, we observed the aggregation of microbiota/fecal metabolites linked to the degree of intestinal inflammation, yielding significant find-

ings in comparisons between HCs vs. BIO and HCs vs. BI1 (Spearman correlation coefficient, SCC absolute value ≥ 0.3 , FDR < 0.05). Significant results of LEfSe analysis were also included in the gut microbiota.

For the “microbiota-blood metabolite-intestinal inflammation” pathway, 40 gut microbiota, 17 metabolite, and intestinal inflammation levels were included (Figure S4). Among them, 13 gut microbes and 10 metabolites were significantly associated with the degree of intestinal inflammation (Figure 5A; the absolute values of the SCC and FDR were ≥ 0.4 and 0.05, respectively). Mediation analysis revealed that 24 out of 35 pathways were significant ($P_{ACME} < 0.05$), and 23 pathways were strongly significant ($P_{ACME} < 0.005$) (Figure 5A). In all 24 significant pathways, the gut microbiota acted as an inhibitor of intestinal inflammation (Figures 5A and S4). For example, the intestinal bacterium *R. gaurvrauii* was negatively correlated with inflammation severity and strongly associated with three blood metabolites, PC(O-34:3), ePE (38:6), and Cer (d18:2/24:2). Mediation analysis also revealed that *R. gaurvrauii* could positively regulate these three blood metabolites, resulting in the inhibition of intestinal

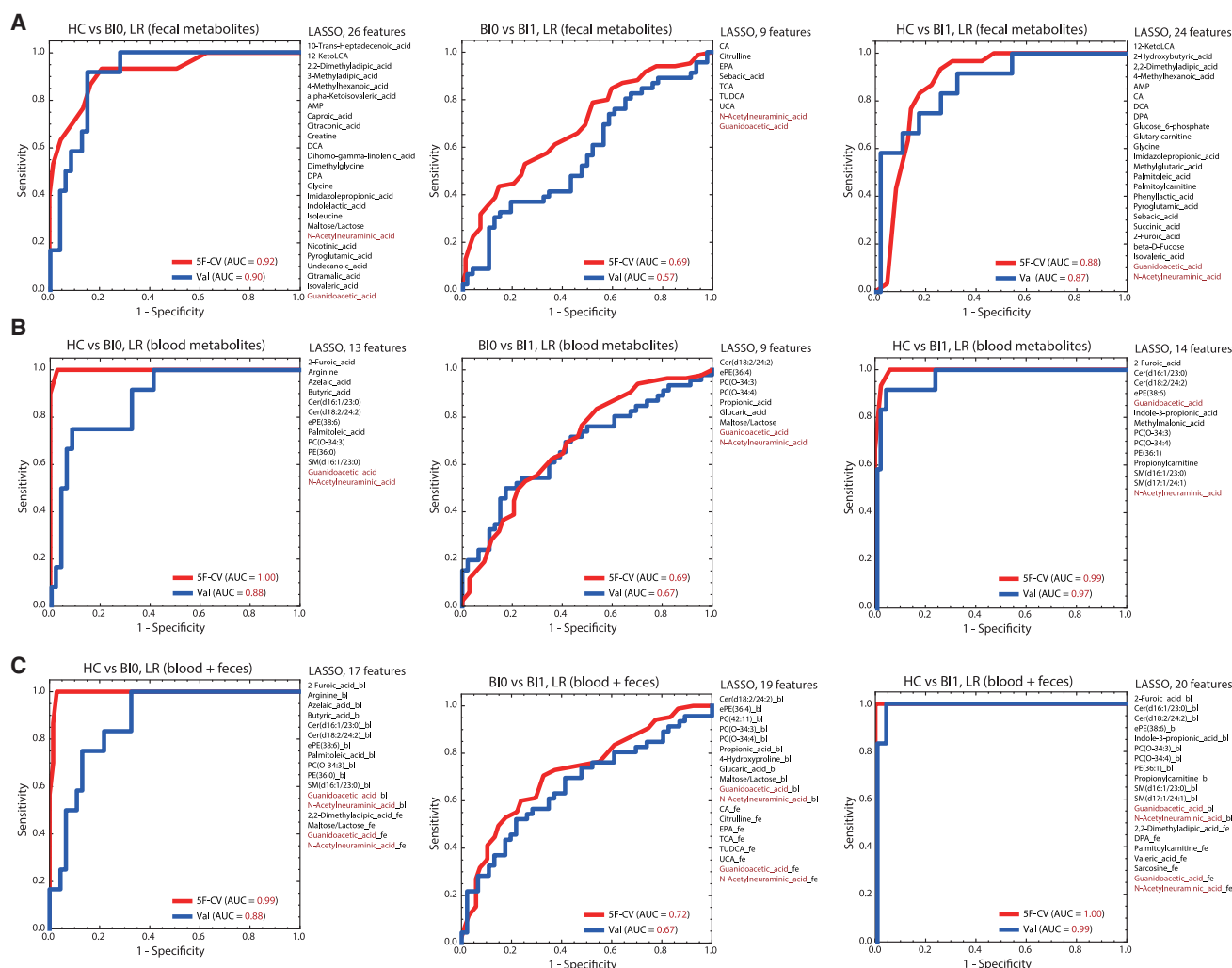


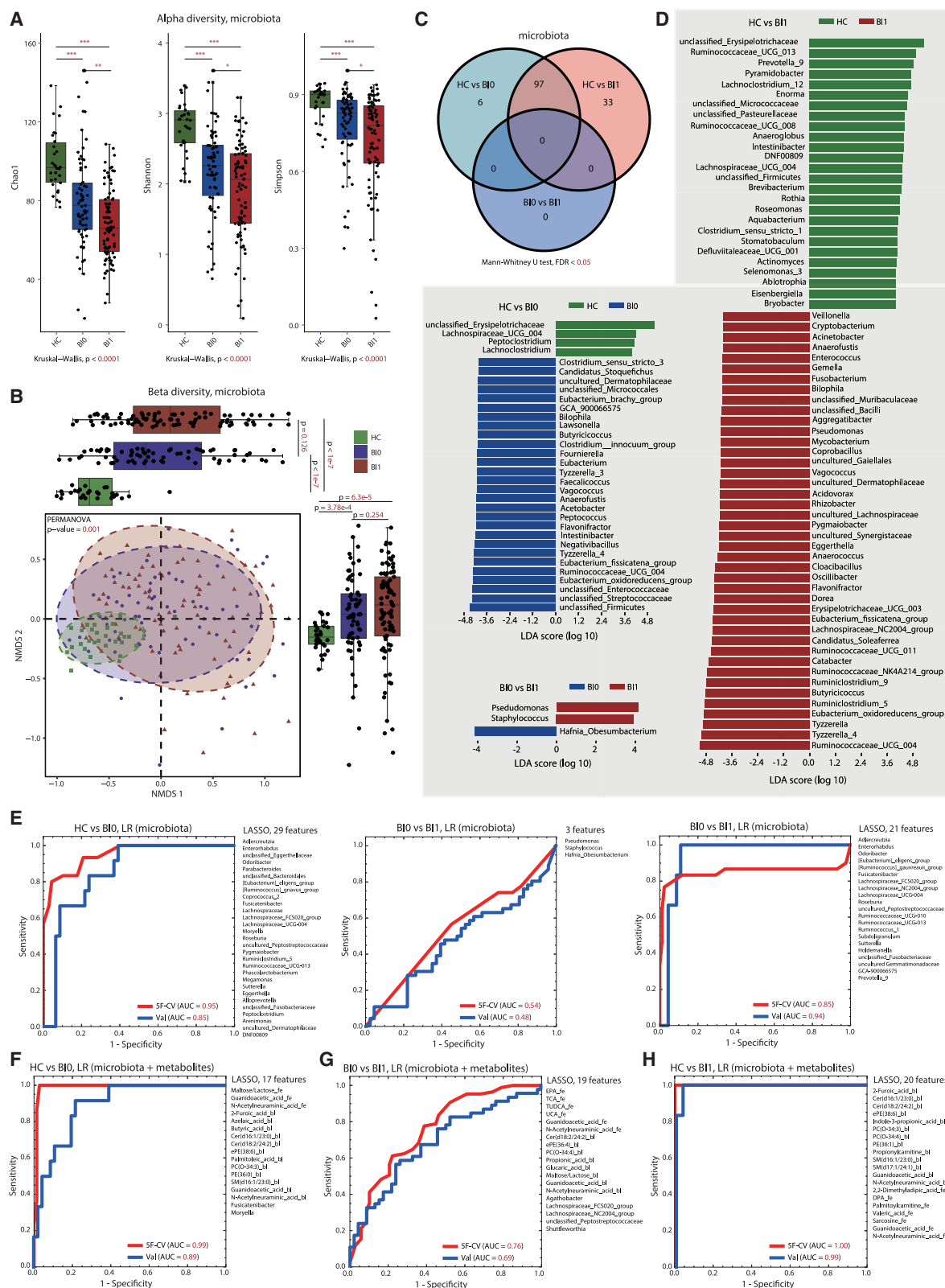
Figure 3. ROC curves of models for the identification of patients with different levels of bowel inflammation based on metabolite-based biomarkers

Models based on the fecal metabolites, blood metabolites, and combined fecal and blood metabolites are shown in (A), (B), and (C), respectively. The features listed on the right of the ROC curves were selected with LASSO regression. Guanidoacetic acid and N-acetylneuraminic acid, shown in red, were always selected as effective biomarkers. Both the 5-fold cross-validation (5F-CV) and the independent validation (Val) results are shown in red and blue, respectively. The rocAUC was indicated for each model, while for 5F-CV evaluation, the mean of 5-fold rocAUC values was indicated. For the models with combinatorial features, the fecal and blood metabolites are indicated by the names followed by ‘_fe’ and ‘_bf’, respectively.

inflammation (Figures 5A and 5B, all $p < 0.05$). The relative abundance of these gut microbes tended to decrease across the BIO and BI1 groups (Figure S5B and S5C).

For the “microbiota-fecal metabolites-intestinal inflammation” pathway, a more complex association network was identified (Figure S6), including 46 gut microbiota and 46 fecal metabolites. Twenty-nine of these gut microbiota presented in blood metabolite pathways. We then selected the most significantly correlated microbiota and metabolites (absolute value of the SCC between the gut microbiota and metabolites ≥ 0.5), including 21 gut microbiota and 25 metabolites (Figure 5C). The bacterial flora and fecal metabolites form complex pathways to regulate inflammation, resulting in a more typical “multibacteria-multimetabolite-intestinal inflammation” pattern. Mediation analysis also

revealed multiple significant pathways ($P_{ACME} < 0.05$), involving the gut microbiota of *Adlercreutzia*, *Odoribacter*, *Alistipes*, *Agathobacter*, and *Fusicatenibacter*; multiple groups of *Lachnospiraceae*, *Roseburia*, *Ruminiclostridium_5* and *Ruminococcaceae*; and metabolites such as 2,2-dimethyladipic acid and 12-ketoLCA (Figure 5C). However, consistent directions were identified in which bacteria correlated with intestinal inflammation directly or by the mediation of metabolites. For example, both *Adlercreutzia* and *Fusicatenibacter* promoted the production of 2,2-dimethyladipic acid in the stool, which mediated the suppression of inflammation (Figure 5D). *Fusicatenibacter* could also positively regulate other inflammation-inhibiting fecal metabolites, such as 12-ketoLCA (Figure 5D). The concentrations of 2,2-dimethyladipic acid and 12-ketoLCA decreased



(legend on next page)

significantly with increasing inflammation (Figure S5D). Surprisingly, *Fusicatenibacter* could also negatively regulate inflammation-promoting blood metabolites such as N-acetylneuraminic acid to inhibit inflammation (Figure 5B).

In summary, the multiple gut microbiota work together to influence inflammation severity by forming complex networks with multiple fecal/blood metabolites.

The gut microbiota and metabolites are correlated with MRE-detectable morphological alterations caused by different intestinal inflammation severity

To noninvasively illustrate the role of the gut microbiota and metabolites in inflammation severity, we further investigated their potential link to intestinal macromorphological alterations. Ten of the 12 MRE findings (Detailed in Table 2), excluding lymph node and perianal disease, exhibited significant correlations with the degree of inflammation ($p < 0.05$). Among these parameters, all but the ADC were positively correlated with the degree of inflammation (Figure 6A).

We then analyzed the correlations between the gut microbiota, metabolites, and MRE features. Twenty-four blood metabolites and four fecal metabolites, but not the gut microbiota, were significantly correlated with ten MRE features (Figures 6A and 6B). These 24 blood metabolites were also included in the 26 subsets that exhibited significant differences between each pair of inflammation groups (Figure 6B). No significant correlation of metabolites with either lymph node alterations or perianal diseases was detected (Figures 6A and S7). Additionally, the lack of significant correlations between microbiota and MREs may be attributed to their relatively lower abundance than that of metabolites.

From the blood and fecal metabolites that were significantly associated with the MRE features (Figure S7), we further identified several significant “metabolite-MRE feature-intestinal inflammation” pathways through mediation analysis (Figure 6C; $P_{ACME} < 0.05$). Most of the metabolites exhibited inverse associations with the MRE features. Among them, blood metabolites were strongly correlated with effusion, thickness, T2WI-SI, and penetration. In particular, N-acetylneuraminic acid, the only blood metabolite identified in this study, significantly promoted inflammation by positively regulating MRE-detectable effusion (Figure 6C). The ADC, the only MRE feature inversely associated with intestinal inflammation, was specifically regulated by guanidinoacetic acid (Figure 6C). Among the fecal metabolites, only citrulline was identified through a “metabolite-MRE feature-intestinal inflammation” pathway, with thickness being the only significant mediating factor (Figure 6C).

Taken together, the associations among the gut microbiota, fecal and blood metabolites, and intestinal/perienteric alterations detected via MRE provide novel evidence supporting the role of these selected multiomics factors in the severity of intestinal inflammation.

DISCUSSION

A recent study revealed that the gut microbiota and its metabolites play important roles in intestinal inflammation.²⁵ We profiled the blood and fecal metabolites and microbiomes of CD patients with different levels of inflammation and compared them with those of HCs, demonstrating that the interactions among CD-associated bacteria and metabolites are altered during the varying levels of intestinal inflammation. Importantly, we expanded on previous research examining the relationship between microbiota, metabolome, and IBD inflammation^{26,27} by further linking microscopic multiomics factors to intestinal macromorphological changes. We demonstrated potential pathways through which bacteria, metabolite markers, and imaging features contribute to different levels of inflammation. This enabled us to identify potential multiomics factors that may lead to increased intestinal inflammation in CD patients.

Previous studies have indicated a strong correlation between the composition of the intestinal microbiota and the incidence of gastrointestinal disorders.^{6,11,28} Our findings revealed that 29 microbiome markers, including various pathogenic bacteria, such as *Alloprevotella*²⁹ and *Roseburia*,¹² had a significant discriminatory effect on BIO patients (rocAUC = 0.89). These BIO patients may be difficult to distinguish from HCs based on imaging features, suggesting the possibility of the use of microecological markers in identifying CD patients with milder inflammatory manifestations.

Moreover, CD patients exhibit characteristic variations in metabolite profiles.¹² Our results demonstrated that the concentration of N-acetylneuraminic acid in the blood and feces gradually increased as inflammation progressed. These findings align with those of previous studies showing a positive correlation with inflammatory markers (e.g., C-reactive protein and sedimentation rate).^{30,31} Interestingly, N-acetylneuraminic acid, a type of sialic acid,³² also serves as a preferential energy source for *Escherichia coli* proliferation. A surge in the *Escherichia coli* population can exacerbate the inflammatory response by inducing the production of proinflammatory cytokines.³³ Moreover, N-acetylneuraminic acid, a proinflammatory factor, was further shown to be significantly negatively correlated with the gut microbiota of *Fusicatenibacter*. The reduction in *Fusicatenibacter*

Figure 4. Different compositions of the gut microbiota between subjects with different levels of bowel inflammation, and ROC curves of models for the classification of patients with different levels of bowel inflammation based on combinatorial biomarkers of metabolites and the gut microbiota

(A and B) Alpha diversity (A) and beta diversity (B) of the gut microbiota of HC, BIO, and BI1 subjects.

(C) Venn diagram showing the number of microbiota taxa with significant differences in relative abundance between the HC, BIO, and BI1 groups.

(D) Gut microbiota with significant differences in relative abundance between the HC, BIO, and BI1 groups detected via LEfSe analysis. All the significant taxa for BIO vs. BI1 are shown. For HCs vs. BIO and HCs vs. BI1, only the taxa with absolute LDA scores ≥ 4.0 are shown, whereas the full sets of significant taxa are shown in Figures S2 and S3.

(E) ROC curves of bowel inflammation prediction models based on the gut microbiota were generated via LASSO regression.

(F–H) The biomarkers were selected via LASSO regression. The fecal and blood metabolites are indicated by ‘_fe’ and ‘_bl’, respectively. The rocAUC was indicated for each model, while for 5F-CV evaluation, the mean of 5-fold rocAUC values was indicated in (E–H).

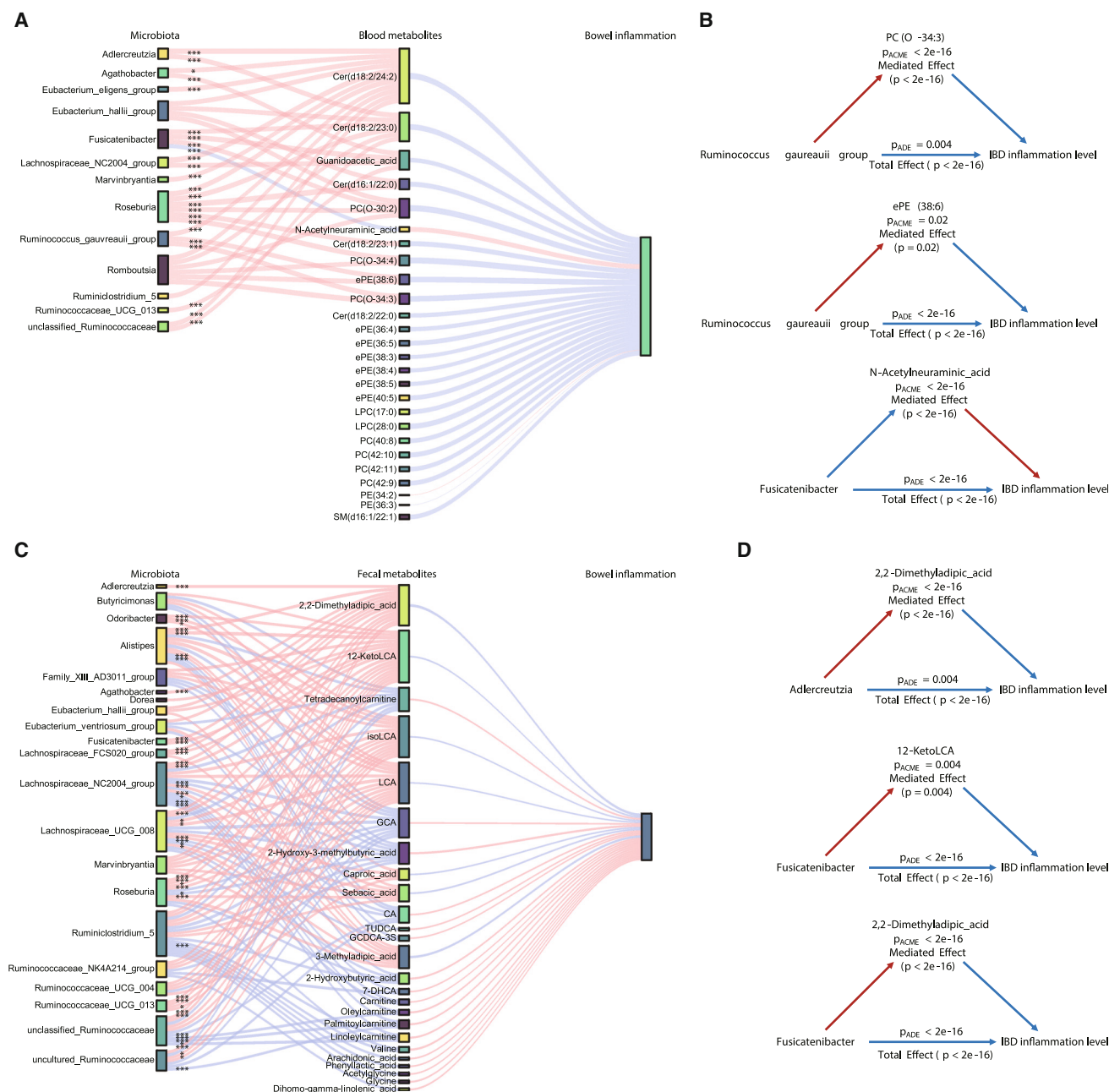


Figure 5. Pathways connected to the gut microbiota, metabolites, and bowel inflammation

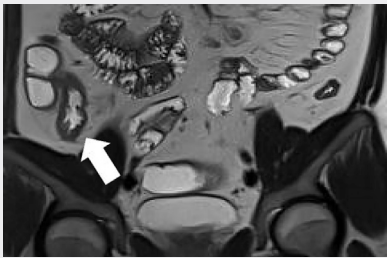

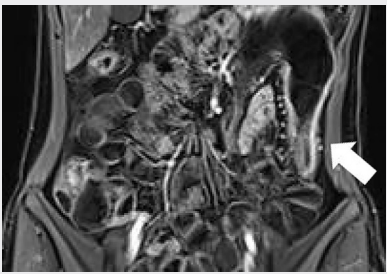
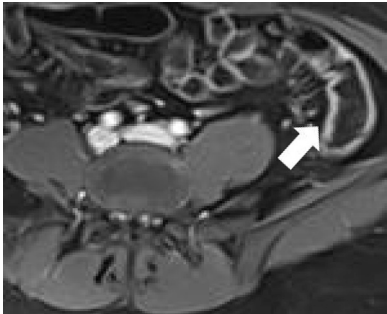
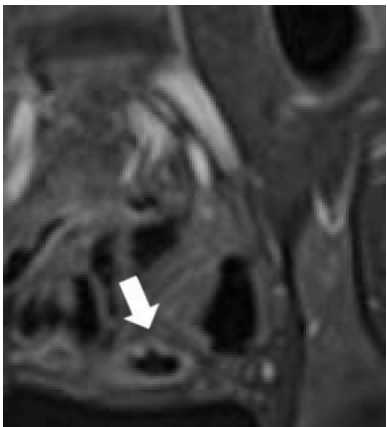
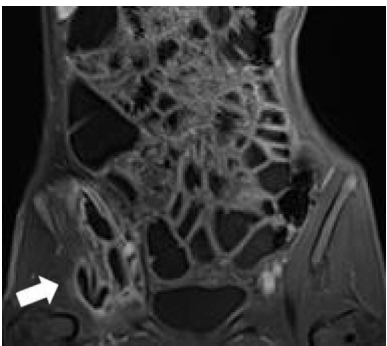
(A) Sankey diagram showing the representative correlation pathways of the gut microbiota, blood metabolites, and bowel inflammation. Only the 26 blood metabolites with significant differences in abundance among all three bowel inflammation groups were identified. The gut microbiota shown in the Sankey diagram is correlated with bowel inflammation ($SCC > 0.3$ or < -0.3 , $FDR < 0.05$) and typically correlated with the listed blood metabolites ($SCC > 0.4$ or < -0.4 , $FDR < 0.05$).

(B) Mediation analysis of the representative pathways of “gut microbiota–blood metabolite–bowel inflammation” (ADE, average direct effect; ACME, average causal mediation effect).

(C) Sankey diagram showing the representative correlation pathways of the gut microbiota, fecal metabolites, and bowel inflammation. The gut bacterial taxa and fecal metabolites shown in the Sankey diagram are correlated with bowel inflammation ($SCC > 0.3$ or < -0.3 , $FDR < 0.05$) and typically correlated with each other ($SCC > 0.5$ or < -0.5 , $FDR < 0.05$).

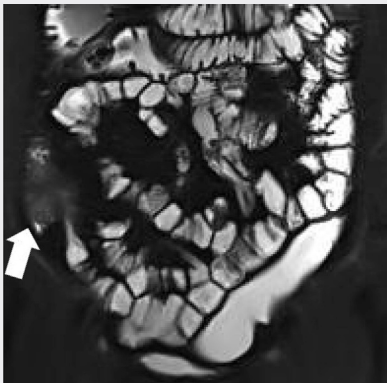
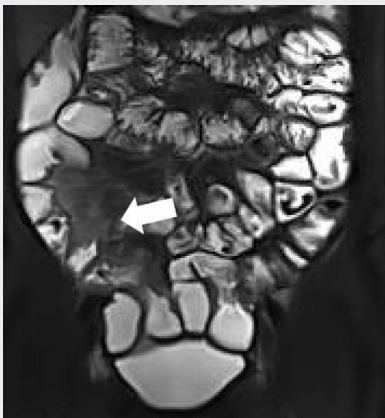
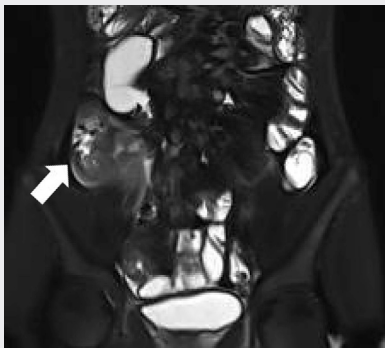
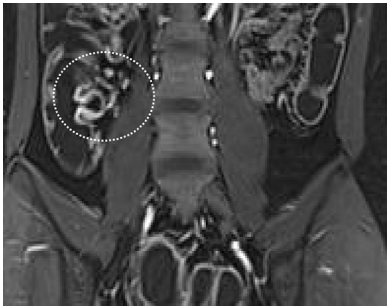

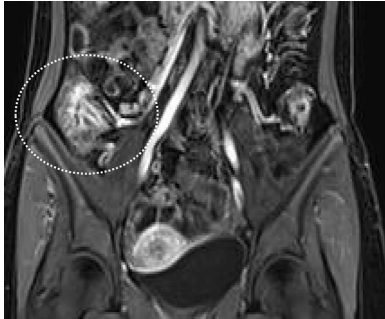


(D) Mediation analysis of the representative pathways of “gut microbiota–faecal metabolite–bowel inflammation”. For (A) and (C), the positive and negative correlations are shown as red and blue lines, respectively, for which the width is proportional to the correlation level. Pathways with significant mediating effects are shown with asterisks. *, significant with p value < 0.05 ; **, significant with p value < 0.01 ; ***, significant with p value < 0.005 .

Table 2. Definitions and illustrations of MRE features

	Score 0	Score 1	Score 2
Semi-quantitative evaluation			
Stricture <ul style="list-style-type: none"> ● Stricture: The bowel diameter is reduced to 50% or less of the adjacent well-expanded normal lumen. ● Pre-stenotic dilatation: The bowel diameter exceeds 1.5 times that of the adjacent well-expanded normal intestinal lumen. 			
	No stricture, no pre-stenotic dilatation	Stricture without pre-stenotic dilatation	Stricture with pre-stenotic dilatation
Penetration <ul style="list-style-type: none"> ● Deep ulcer: Thickened intestinal mucosa interruptions cause contrast agent infiltration into the serosa, yielding thin linear high-signal patterns on T₂-weighted imaging. ● Fistula: Abnormal channels were observed connecting the affected bowel to other bowel segments, body cavities, or the body surface, including bowel-bowel fistula, bowel-cutaneous fistula, intestinal-bladder fistula as well as intestinal-vaginal fistula. ● Abscess: mesenteric or peritoneal fluid collection with rim enhancement and/or internal air. 			
	No penetration	Deep ulcer	Fistula/abscess


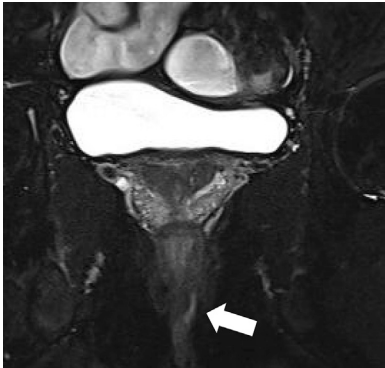
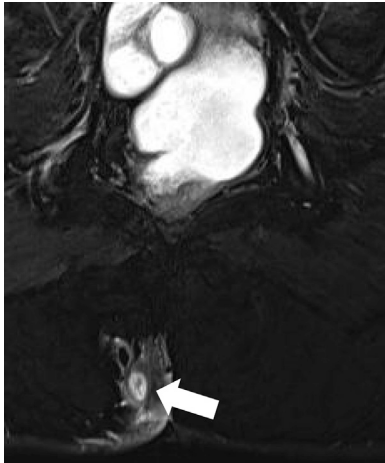
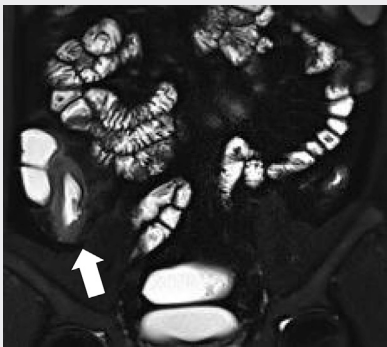
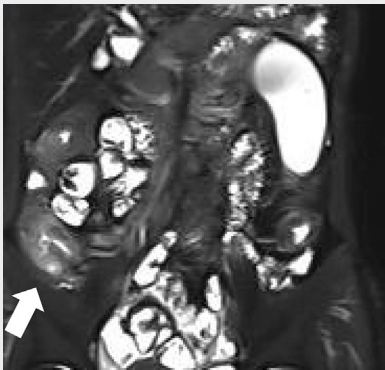
(Continued on next page)

Table 2. Continued

	Score 0	Score 1	Score 2
Effusion The increase of perienteric signal on fat-suppressed T2WI sequence with or without perienteric effusion was observed.	 Similar to the normal mesentery	 Increased mesenteric signal without perienteric effusion	 Increased mesenteric signal with perienteric effusion
Bowel wall contrast enhancement (CE) extent The enhancement extent in the arterial phase of the affected bowel wall was compared with that of the normal bowel wall and blood vessels.	 Similar to the normal bowel	 Stronger than that of normal bowel wall but weaker than that of adjacent vessels	 Close to the adjacent blood vessels
Bowel wall contrast enhancement (CE) pattern	 Homogeneous enhancement throughout the entire layer	 Mucosal enhancement exceeded submucosal, muscular, and serous layers	/

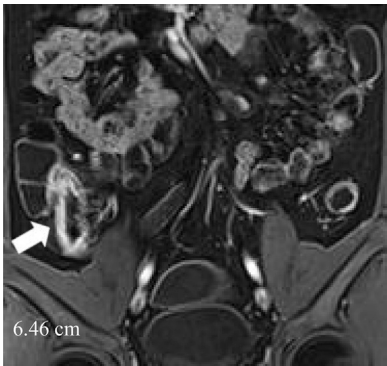
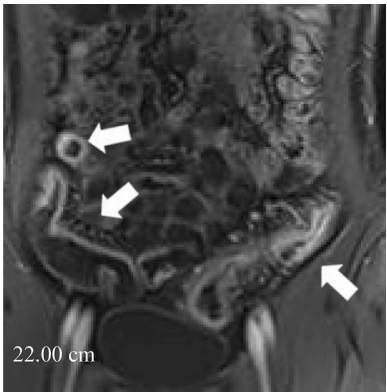
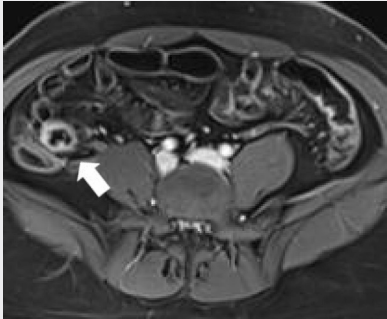
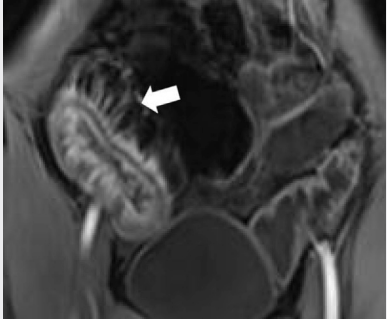
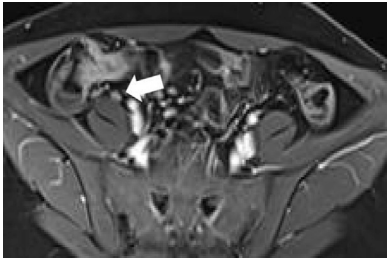
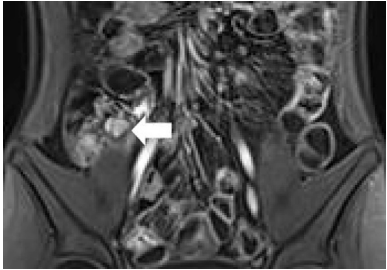
(Continued on next page)

Table 2. Continued

	Score 0	Score 1	Score 2
Perianal diseases	 <p>No perianal diseases</p>	 <p>Perianal fistula</p>	 <p>Perianal abscess</p>
Bowel wall T2WI signal (T2WI-SI) The bowel wall signal on the T ₂ W non-fat sequence was measured when the bowel cavity was well filled.	 <p>Similar to the normal bowel wall</p>	 <p>Higher than the normal bowel</p>	


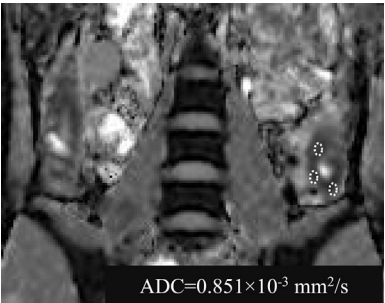
(Continued on next page)

Table 2. Continued

	Score 0	Score 1	Score 2
Length of diseased bowel The length of the bowel segment with the most obvious lesion was comprehensively evaluated in combination with multiple directions.	 Length ≤15 cm	 Length >15 cm	/
Comb sign The vessels on the mesenteric side of the affected bowel were dilated and arranged in comb shape, which was observed on the enhanced arterial phase.	 No comb sign	 Comb sign	/
Lymph node	 Short axis of lymph node ≤10 mm	 Short axis of lymph node >10 mm	/

(Continued on next page)

Table 2. Continued

	Score 0	Score 1	Score 2
Quantitative evaluation			
Bowel wall thickness Measured the largest bowel wall thickness on the thickest area on the short axis of inflamed intestine			
Bowel wall ADC ($\times 10^{-3}$ mm²/s) The region of interest covered the affected bowel wall and the delineation of extraenteric structures was avoided.			
Note. MRE, magnetic resonance enterography; T ₂ WI, T ₂ weighted imaging; ADC, apparent diffusion coefficient.			

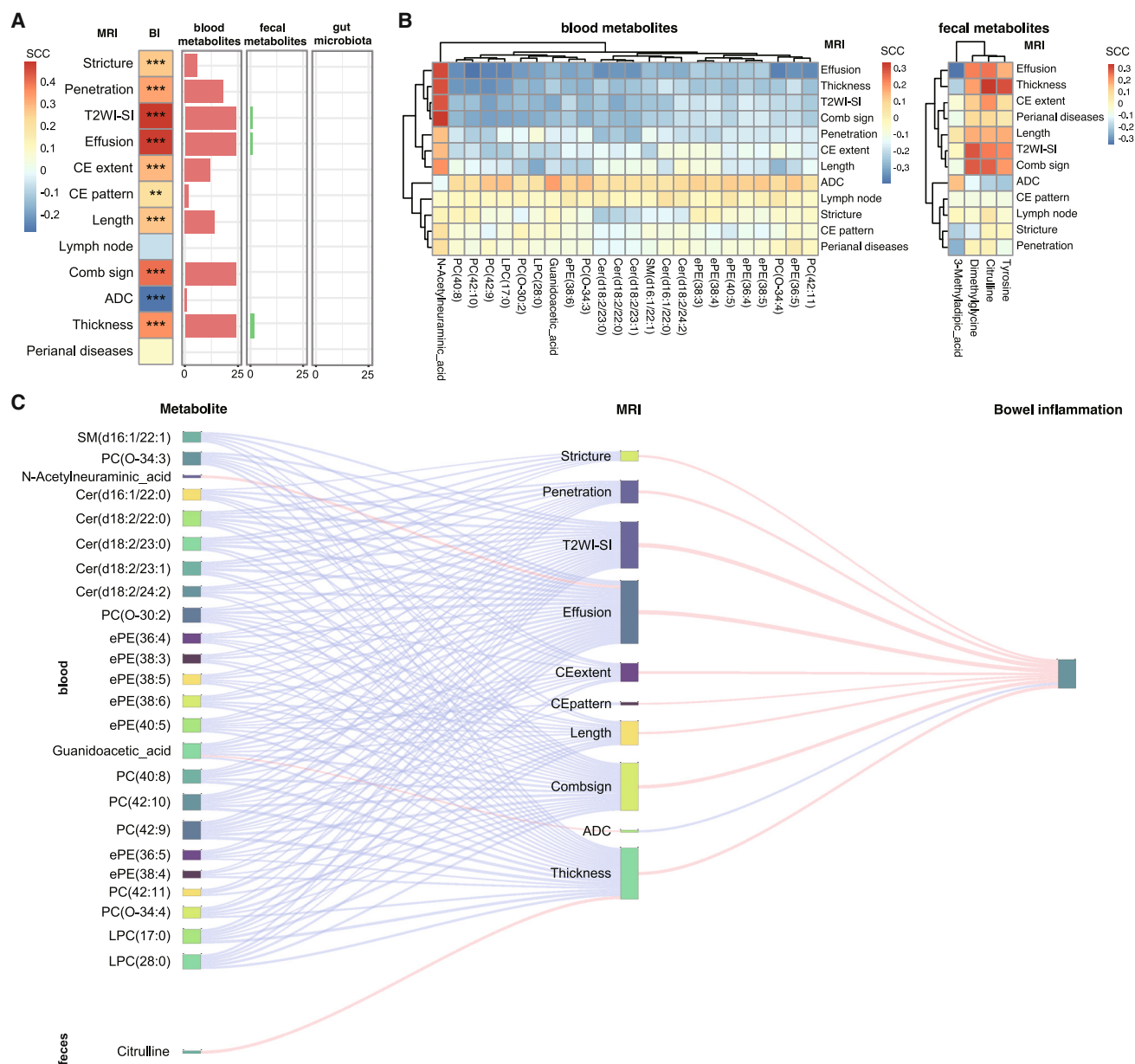


Figure 6. Correlations between MRI findings and bowel inflammation, metabolites, or the gut microbiota

(A) Spearman correlations between the twelve MRI features and bowel inflammation (BI) or biological factors. The MRI features that were significantly correlated with the BI are shown with asterisks. *, significant with p value <0.05 ; **, significant with p value <0.01 ; ***, significant with p value <0.005 . The numbers of metabolites and gut microbes significantly correlated with the MRI features are shown in bar plots.

(B) Heatmaps illustrating the SCC between representative blood or fecal metabolites and MRI indications. The representative blood metabolites presented significant differences in abundance among all three groups and were significantly correlated with at least one of the twelve MRI features. The fecal metabolites were significantly correlated with both the BI and at least one of the twelve MRI features.

(C) Sankey diagram showing the pathways associated with metabolites, MRI features, and bowel inflammation. All the metabolites were significantly correlated with BI. Only the pathways with significant mediating effects according to the MRI features are shown. The positive and negative correlations are shown as red and blue lines, respectively, for which the width is proportional to the correlation level.

may contribute to the increase in C-reactive protein levels in CD patients.³⁴ The presence of *Fusicatenibacter* is inversely correlated with intestinal inflammation and exerts inhibitory effects on N-acetylneuraminic acid, thereby exerting a suppressive effect on overall intestinal inflammation. Additionally, this study re-

vealed that *Ruminococcus gnavreus* had a low abundance in CD, whereas *R. gnavus* had a high abundance; although both showed a decreasing trend from BI0 to BI1, they had opposite effects on inflammation through metabolites (Figures S5B and S5C). Moreover, our LefSe analysis revealed that the abundance

of *Pseudomonas* and *Staphylococcus* increased from BI0 to BI1, indicating an inducing effect of inflammation. Current studies have also demonstrated that lipopolysaccharide release from *Pseudomonas* activates NF- κ B signaling, leading to inflammation.³⁵ Moreover, *Staphylococcus* produces serine protease-like proteins associated with allergic inflammation.³⁶

In addition to N-acetylneuraminic acid, 26 blood lipid metabolites varied significantly across inflammation processes. Ceramides are crucial for various cellular physiological processes, including stress and inflammation.³⁷ However, the impact of ceramides with different acyl chain lengths on IBD remains unexplored.³⁸ Preclinical studies have shown that ceramide liposomes can alleviate colitis in IBD mice.³⁹ These findings support our observation that ceramide levels tended to decrease from HCs to CD patients with variance in inflammation. Additionally, diminished levels of phosphatidylcholine (PC) are associated with the onset of inflammation.⁴⁰ By modulating lysophosphatidylcholine metabolism, it is possible to mitigate inflammation and enhance intestinal barrier function,⁴¹ supporting our findings.

To elucidate the underlying mechanism responsible for the generation of characteristic metabolites, KEGG pathway analysis was employed to reveal differential pathways. The ether lipid metabolism pathway and sphingolipid metabolic pathway were significantly altered in moderate-to-severe CD-related inflammation, which aligns with the findings of previous studies.⁴² Another study reported that host sphingolipid levels are correlated with the inflammatory effect of fecal bacteroides.⁴³ Moreover, the ether lipid metabolism pathway induces inflammation progression through regulating neutrophil accumulation.⁴⁴ With respect to the fecal metabolic pathways, glycine, serine, and threonine metabolism pathways were enriched in the moderate-to-severe inflammatory group, which aligns with the findings of an IBD mouse experiment.⁴⁵

In clinical practice, MRI is a valuable reference for surgical decision-making in CD patients because it allows accurate identification of imaging features such as stenosis or penetration.^{46,47} According to the European Crohn's and Colitis Organisation (ECCO) guidelines, a comprehensive assessment of the intestines, ideally via preoperative MRE, is crucial when surgical intervention becomes necessary.⁴⁸ Therefore, we also identified a significant correlation between microscopic metabolic markers and macroscopic imaging features, suggesting the involvement of multiple metabolites in the inflammatory process underlying these imaging features. Most blood metabolites, including N-acetylneuraminic acid, guanidinoacetic acid, and ceramide, that persist in varying levels of inflammation have inhibitory effects on imaging features associated with the degree of inflammation. This finding offers additional information for personalized precision medicine to delay or prevent severe inflammation.

In conclusion, our comprehensive investigation of the gut microbiome and metabolites revealed dynamic alterations in specific components associated with different levels of intestinal inflammation, highlighting the potential association between the gut microbiota, metabolites, and intestinal inflammation severity. We also established a link between microscopic microbiota metabolite markers and macroscopic imaging features.

Modulating crucial microbial metabolites could mitigate the pronounced inflammation associated with imaging features, thereby circumventing the need for surgery. Additionally, we primarily employed mediation analysis to establish the causal relationship between microscopic and macroscopic factors, thereby facilitating the identification of more specific biomarkers. In the future, alternative causality analysis methods such as Mendelian randomization could be considered for more robust results.

Limitations of the study

There are certain limitations in our study. First, this was a single-center study. However, the participants were recruited from a highly reputable IBD center with wide geographical representation. This highlights the study's commitment to population diversity and encourages model generalizability. In the future, including data from other centers could further increase the robustness and replicability of our conclusions. Second, we could not track the same patient over time or collect multiomics data at different intervals, which would demonstrate the dynamic changes in these omics data with intestinal inflammation within an individual's body. Third, *in vivo* animal experiments were not performed. Finally, we used traditional MRE sequences for evaluating intestinal stricture features, which may not accurately differentiate inflammatory from fibrotic strictures.⁴⁹ Future studies should consider employing advanced MRI techniques, such as magnetization transfer imaging, or using excised intestinal specimens as histological controls to more precisely distinguish the stricture types. This would enable a more thorough evaluation of the differences in microbiota and metabolomics between these two types of strictures.

RESOURCE AVAILABILITY

Lead contact

Further information and requests should be directed to the lead contact, Prof. Xue-Hua Li (xueh@mail.sysu.edu.cn).

Materials availability

This study did not generate new unique reagents.

Data and code availability

All data reported in this paper will be shared by the [lead contact](#) upon request.

This paper does not report any original code.

Any additional information required to reanalyze the data reported in this paper is available from the [lead contact](#) upon request.

ACKNOWLEDGMENTS

This study was financially supported by National Natural Science Foundation of China (82270693, 82070680, 82271958, 82471948, 82072002, 81970483, 82170537, and 82222010), Guangdong Basic and Applied Basic Research Foundation (2023B1515020070, 2023A1515011097, 2023A1515010388, and 2023A1515011304), Fundamental Research Funds for the Central Universities, Sun Yat-sen University (24ykqb003), 2023 SKY Imaging Research Fund of the Chinese International Medical Foundation (Z-2014-07-2301), National Key R&D Program of China (2023YFC2507300), Key Area Research and Development Program of Guangdong Province (2023B1111040003), National Undergraduate Training Program of China for Innovation and Entrepreneurship (202410590053). The funders of the study had no role in study design, data collection, data analysis, data interpretation, or writing of the report.

AUTHOR CONTRIBUTIONS

R.-N.Z., Z.-L.L., and L.H.: guarantor, design, data analysis, preparation, editing, and review; W.-M.K., Y.-D.Z., Y.-D.W., X.-D.S., L.-L.H., X.-Y.W., Q.-Z.Z., L.-Y.W., Y.-Q.K., R.M., Z.-P.P., C.-H.S., and S.-T.F.: concepts, experimental studies, data analysis, preparation, editing, and review; S.-C.L., Y.-J.W., and X.-H.L.: guarantor, concepts, design, data analysis, preparation, editing, and review. All authors read and approved for the final manuscript.

DECLARATION OF INTERESTS

The authors declare no competing interests.

STAR★METHODS

Detailed methods are provided in the online version of this paper and include the following:

- **KEY RESOURCES TABLE**
- **EXPERIMENTAL MODEL AND STUDY PARTICIPANT DETAILS**
 - Ethics statement
 - Patient recruitment and specimen collection
- **METHOD DETAILS**
 - Grading intestinal inflammation via MRE and ileocolonoscopy
 - Assessment of intestinal inflammation-associated morphological alterations on MRE
 - Faecal and blood metabolomics
 - 16S rRNA gene amplicon sequencing
- **QUANTIFICATION AND STATISTICAL ANALYSIS**

SUPPLEMENTAL INFORMATION

Supplemental information can be found online at <https://doi.org/10.1016/j.isci.2025.112310>.

Received: November 16, 2024

Revised: February 6, 2025

Accepted: March 25, 2025

Published: March 28, 2025

REFERENCES

1. GBD 2017 Inflammatory Bowel Disease Collaborators (2020). The global, regional, and national burden of inflammatory bowel disease in 195 countries and territories, 1990–2017: a systematic analysis for the Global Burden of Disease Study 2017. *Lancet Gastroenterol Hepatol.* 5, 17–30. [https://doi.org/10.1016/S2468-1253\(19\)30333-4](https://doi.org/10.1016/S2468-1253(19)30333-4).
2. Morgan, X.C., Tickle, T.L., Sokol, H., Gevers, D., Devaney, K.L., Ward, D.V., Reyes, J.A., Shah, S.A., LeLeiko, N., Snapper, S.B., et al. (2012). Dysfunction of the intestinal microbiome in inflammatory bowel disease and treatment. *Genome Biol.* 13, R79. <https://doi.org/10.1186/gb-2012-13-9-r79>.
3. Knights, D., Silverberg, M.S., Weersma, R.K., Gevers, D., Dijkstra, G., Huang, H., Tyler, A.D., van Sommeren, S., Imhann, F., Stempak, J.M., et al. (2014). Complex host genetics influence the microbiome in inflammatory bowel disease. *Genome Med.* 6, 107. <https://doi.org/10.1186/s13073-014-0107-1>.
4. Pollok, R.C.G., and Jayasooriya, N. (2022). Editorial: early and persistent biological treatment and its impact on long term surgical outcomes in inflammatory bowel disease. *Aliment. Pharmacol. Ther.* 55, 370–371. <https://doi.org/10.1111/apt.16747>.
5. Witte, M., Reiner, J., Bannert, K., Jaster, R., Maschmeier, C., Schafmayer, C., Lamprecht, G., and Berlin, P. (2021). Ileocolonic Healing After Extended Small Bowel Resection in Mice: NOD2 Deficiency Impairs Anastomotic Healing and Postoperative Outcome. *Inflamm. Bowel Dis.* 27, 1503–1512. <https://doi.org/10.1093/ibd/izab022>.
6. Degenhardt, F., Dirmeier, A., Lopez, R., Lang, S., Kunst, C., Roggenbuck, D., Reinhold, D., Szymczak, S., Rogler, G., Klebl, F., et al. (2016). Serologic Anti-GP2 Antibodies Are Associated with Genetic Polymorphisms, Fibrosinosis, and Need for Surgical Resection in Crohn's Disease. *Inflamm. Bowel Dis.* 22, 2648–2657.
7. Rivi re, P., Bislenghi, G., Hammoudi, N., Verstockt, B., Brown, S., Oliveira-Cunha, M., Bemelman, W., Pellino, G., Kotze, P.G., 8th Scientific Workshop of the European Crohn's and Colitis Organisation, et al. (2023). Results of the Eighth Scientific Workshop of ECCO: Pathophysiology and Risk Factors of Postoperative Crohn's Disease Recurrence after an Ileocolonic Resection. *J. Crohns Colitis* 17, 1557–1568. <https://doi.org/10.1093/ecco-jcc/ijad054>.
8. Lavelle, A., and Sokol, H. (2020). Gut microbiota-derived metabolites as key actors in inflammatory bowel disease. *Nat. Rev. Gastroenterol. Hepatol.* 17, 223–237. <https://doi.org/10.1038/s41575-019-0258-z>.
9. Wang, C., Gu, Y., Chu, Q., Wang, X., Ding, Y., Qin, X., Liu, T., Wang, S., Liu, X., Wang, B., and Cao, H. (2024). Gut microbiota and metabolites as predictors of biologics response in inflammatory bowel disease: A comprehensive systematic review. *Microbiol. Res.* 282, 127660. <https://doi.org/10.1016/j.micres.2024.127660>.
10. Spathakis, M., Dovrolis, N., Filidou, E., Kandilogiannakis, L., Tarapatzi, G., Valatas, V., Drygiannakis, I., Paspaliaris, V., Arvanitidis, K., Manolopoulos, V.G., et al. (2024). Exploring Microbial Metabolite Receptors in Inflammatory Bowel Disease: An In Silico Analysis of Their Potential Role in Inflammation and Fibrosis. *Pharmaceuticals* 17, 492. <https://doi.org/10.3390/ph17040492>.
11. Lloyd-Price, J., Arze, C., Ananthakrishnan, A.N., Schirmer, M., Avila-Pacheco, J., Poon, T.W., Andrews, E., Ajami, N.J., Bonham, K.S., Brislawn, C.J., et al. (2019). Multi-omics of the gut microbial ecosystem in inflammatory bowel diseases. *Nature* 569, 655–662. <https://doi.org/10.1038/s41586-019-1237-9>.
12. Franzosa, E.A., Sirota-Madi, A., Avila-Pacheco, J., Fornelos, N., Haiser, H.J., Reinker, S., Vatanen, T., Hall, A.B., Mallick, H., McIver, L.J., et al. (2019). Gut microbiome structure and metabolic activity in inflammatory bowel disease. *Nat. Microbiol.* 4, 293–305. <https://doi.org/10.1038/s41564-018-0306-4>.
13. Santoru, M.L., Piras, C., Murgia, A., Palmas, V., Camboni, T., Liggi, S., Ibba, I., Lai, M.A., Orr , S., Blois, S., et al. (2017). Cross sectional evaluation of the gut-microbiome metabolome axis in an Italian cohort of IBD patients. *Sci. Rep.* 7, 9523. <https://doi.org/10.1038/s41598-017-10034-5>.
14. Marchesi, J.R., Holmes, E., Khan, F., Kochhar, S., Scanlan, P., Shanahan, F., Wilson, I.D., and Wang, Y. (2007). Rapid and noninvasive metabonomic characterization of inflammatory bowel disease. *J. Proteome Res.* 6, 546–551.
15. Nikolaus, S., Schulte, B., Al-Massad, N., Thieme, F., Schulte, D.M., Bethge, J., Rehman, A., Tran, F., Aden, K., H sler, R., et al. (2017). Increased Tryptophan Metabolism Is Associated With Activity of Inflammatory Bowel Diseases. *Gastroenterology* 153, 1504–1516.e2. <https://doi.org/10.1053/j.gastro.2017.08.028>.
16. Rimola, J., Torres, J., Kumar, S., Taylor, S.A., and Kucharzik, T. (2022). Recent advances in clinical practice: advances in cross-sectional imaging in inflammatory bowel disease. *Gut* 71, 2587–2597. <https://doi.org/10.1136/gutjnl-2021-326562>.
17. Hameed, M., Kumar, S., and Taylor, S.A. (2025). How I Do It: Cross-sectional Imaging in Small-Bowel Crohn Disease and Ulcerative Colitis. *Radiology* 314, e241452. <https://doi.org/10.1148/radiol.241452>.
18. Pokala, A., and Shen, B. (2020). Update of endoscopic management of Crohn's disease strictures. *Intest. Res.* 18, 1–10. <https://doi.org/10.5217/ir.2019.09158>.
19. Daperno, M., D'Haens, G., Van Assche, G., Baert, F., Bulois, P., Maunoury, V., Sostegni, R., Rocca, R., Pera, A., Gevers, A., et al. (2004). Development and validation of a new, simplified endoscopic activity score for Crohn's disease: the SES-CD. *Gastrointest. Endosc.* 60, 505–512.

20. Kumar, S., De Kock, I., Blad, W., Hare, R., Pollok, R., and Taylor, S.A. (2024). Magnetic Resonance Enterography and Intestinal Ultrasound for the Assessment and Monitoring of Crohn's Disease. *J. Crohns Colitis* 18, 1450–1463. <https://doi.org/10.1093/ecco-jcc/jjae042>.
21. Lacotte, E., Boujonnier, L., Martinez-Vinson, C., Viala, J., Ley, D., Coopman, S., Lerisson, H., Dabadie, A., Dumant-Forrest, C., Pigneur, B., et al. (2024). Risk factors for surgery in stricturing small bowel Crohn's disease: A retrospective cohort study from the GETAID pédiatrique. *J. Pediatr. Gastroenterol. Nutr.* 78, 1261–1272. <https://doi.org/10.1002/jpn3.12224>.
22. Lin, C.K., and Kazmierczak, B.I. (2017). Inflammation: A Double-Edged Sword in the Response to *Pseudomonas aeruginosa* Infection. *J. Innate Immun.* 9, 250–261. <https://doi.org/10.1159/000455857>.
23. Scales, B.S., Dickson, R.P., LiPuma, J.J., and Huffnagle, G.B. (2014). Microbiology, genomics, and clinical significance of the *Pseudomonas fluorescens* species complex, an unappreciated colonizer of humans. *Clin. Microbiol. Rev.* 27, 927–948. <https://doi.org/10.1128/CMR.00044-14>.
24. Kaelin, E.A., Rodriguez, C., Hall-Moore, C., Hoffmann, J.A., Linneman, L.A., Ndao, I.M., Warner, B.B., Tarr, P.I., Holtz, L.R., and Lim, E.S. (2022). Longitudinal gut virome analysis identifies specific viral signatures that precede necrotizing enterocolitis onset in preterm infants. *Nat. Microbiol.* 7, 653–662. <https://doi.org/10.1038/s41564-022-01096-x>.
25. Kakhana, K., Fujioka, Y., Suda, W., Najima, Y., Kuwata, G., Sasajima, S., Mimura, I., Morita, H., Sugiyama, D., Nishikawa, H., et al. (2016). Fecal microbiota transplantation for patients with steroid-resistant acute graft-versus-host disease of the gut. *Blood* 128, 2083–2088. <https://doi.org/10.1182/blood-2016-05-717652>.
26. Metwaly, A., Dunkel, A., Waldschmitt, N., Raj, A.C.D., Lagkouvardos, I., Corraliza, A.M., Mayorgas, A., Martinez-Medina, M., Reiter, S., Schlöter, M., et al. (2020). Integrated microbiota and metabolite profiles link Crohn's disease to sulfur metabolism. *Nat. Commun.* 11, 4322. <https://doi.org/10.1038/s41467-020-17956-1>.
27. Ning, L., Zhou, Y.-L., Sun, H., Zhang, Y., Shen, C., Wang, Z., Xuan, B., Zhao, Y., Ma, Y., Yan, Y., et al. (2023). Microbiome and metabolome features in inflammatory bowel disease via multi-omics integration analyses across cohorts. *Nat. Commun.* 14, 7135. <https://doi.org/10.1038/s41467-023-42788-0>.
28. Jomehzadeh, N., Javaherizadeh, H., Amin, M., Saki, M., Al-Ouqailli, M.T.S., Hamidi, H., Seyedmahmoudi, M., and Gorjian, Z. (2020). Isolation and identification of potential probiotic *Lactobacillus* species from feces of infants in southwest Iran. *Int. J. Infect. Dis.* 96, 524–530. <https://doi.org/10.1016/j.ijid.2020.05.034>.
29. Wang, C., Li, W., Wang, H., Ma, Y., Zhao, X., Zhang, X., Yang, H., Qian, J., and Li, J. (2019). *Saccharomyces boulardii* alleviates ulcerative colitis carcinogenesis in mice by reducing TNF- α and IL-6 levels and functions and by rebalancing intestinal microbiota. *BMC Microbiol.* 19, 246. <https://doi.org/10.1186/s12866-019-1610-8>.
30. Wu, E.B., Lumb, P., Chambers, J.B., and Crook, M.A. (1999). Plasma sialic acid and coronary artery atheromatous load in patients with stable chest pain. *Atherosclerosis* 145, 261–266.
31. Crook, M.A., Haq, M., and Tutt, P. (1997). Serum sialic acid and its relationship to various haematological parameters, including erythrocyte sedimentation rate. *Br. J. Biomed. Sci.* 54, 100–103.
32. Yida, Z., Imam, M.U., Ismail, M., Ismail, N., Ideris, A., and Abdullah, M.A. (2015). High fat diet-induced inflammation and oxidative stress are attenuated by N-acetylneuraminic acid in rats. *J. Biomed. Sci.* 22, 96. <https://doi.org/10.1186/s12929-015-0211-6>.
33. Huang, Y.-L., Chassard, C., Hausmann, M., von Itzstein, M., and Hennot, T. (2015). Sialic acid catabolism drives intestinal inflammation and microbial dysbiosis in mice. *Nat. Commun.* 6, 8141. <https://doi.org/10.1038/ncomms9141>.
34. Essex, M., Rios Rodriguez, V., Rademacher, J., Proft, F., Löber, U., Markó, L., Pleyer, U., Strowig, T., Marchand, J., Kirwan, J.A., et al. (2024). Shared and Distinct Gut Microbiota in Spondyloarthritis, Acute Anterior Uveitis, and Crohn's Disease. *Arthritis Rheumatol.* 76, 48–58. <https://doi.org/10.1002/art.42658>.
35. Li, J., Li, Y., Zhou, L., Li, H., Wan, T., Tang, J., Zhou, L., Xie, H., and Wang, L. (2024). Microbiome analysis reveals the inducing effect of *Pseudomonas* on prostatic hyperplasia via activating NF- κ B signalling. *Virulence* 15, 2313410. <https://doi.org/10.1080/21505594.2024.2313410>.
36. De Donato, D.P., Effner, R., Nordengrün, M., Lechner, A., Darisipudi, M.N., Volz, T., Hagl, B., Bröker, B.M., and Renner, E.D. (2024). *Staphylococcus aureus* Serine protease-like protein A (SplA) induces IL-8 by keratinocytes and synergizes with IL-17A. *Cytokine* 180, 156634. <https://doi.org/10.1016/j.cyto.2024.156634>.
37. Buccoliero, R., and Futerman, A.H. (2003). The roles of ceramide and complex sphingolipids in neuronal cell function. *Pharmacol. Res.* 47, 409–419.
38. Kim, Y.-R., Volpert, G., Shin, K.-O., Kim, S.-Y., Shin, S.-H., Lee, Y., Sung, S.H., Lee, Y.-M., Ahn, J.-H., Pewzner-Jung, Y., et al. (2017). Ablation of ceramide synthase 2 exacerbates dextran sodium sulphate-induced colitis in mice due to increased intestinal permeability. *J. Cell Mol. Med.* 21, 3565–3578. <https://doi.org/10.1111/jcmm.13267>.
39. Matsukawa, T., Izawa, K., Isobe, M., Takahashi, M., Maehara, A., Yamashita, Y., Kaitani, A., Okumura, K., Teshima, T., Kitamura, T., and Kitaura, J. (2016). Ceramide-CD300f binding suppresses experimental colitis by inhibiting ATP-mediated mast cell activation. *Gut* 65, 777–787. <https://doi.org/10.1136/gutjnl-2014-308900>.
40. Arendt, B.M., Ma, D.W.L., Simons, B., Noureldin, S.A., Therapondos, G., Guindi, M., Sherman, M., and Allard, J.P. (2013). Nonalcoholic fatty liver disease is associated with lower hepatic and erythrocyte ratios of phosphatidylcholine to phosphatidylethanolamine. *Appl. Physiol. Nutr. Metab.* 38, 334–340. <https://doi.org/10.1139/apnm-2012-0261>.
41. Gao, D., Zhao, H., Yin, Z., Han, C., Wang, Y., Luo, G., and Gao, X. (2021). Rheum tanguticum Alleviates Cognitive Impairment in APP/PS1 Mice by Regulating Drug-Responsive Bacteria and Their Corresponding Microbial Metabolites. *Front. Pharmacol.* 12, 766120. <https://doi.org/10.3389/fphar.2021.766120>.
42. Fischbeck, A., Leucht, K., Frey-Wagner, I., Bentz, S., Pesch, T., Kellermeier, S., Krebs, M., Fried, M., Rogler, G., Hausmann, M., and Humpf, H.-U. (2011). Sphingomyelin induces cathepsin D-mediated apoptosis in intestinal epithelial cells and increases inflammation in DSS colitis. *Gut* 60, 55–65. <https://doi.org/10.1136/gut.2009.201988>.
43. Brown, E.M., Ke, X., Hitchcock, D., Jeanfavre, S., Avila-Pacheco, J., Nakata, T., Arthur, T.D., Fornelos, N., Heim, C., Franzosa, E.A., et al. (2019). Bacteroides-Derived Sphingolipids Are Critical for Maintaining Intestinal Homeostasis and Symbiosis. *Cell Host Microbe* 25, 668–680.e7. <https://doi.org/10.1016/j.chom.2019.04.002>.
44. Lodhi, I.J., Wei, X., Yin, L., Feng, C., Adak, S., Abou-Ezzi, G., Hsu, F.-F., Link, D.C., and Semenkovich, C.F. (2015). Peroxisomal lipid synthesis regulates inflammation by sustaining neutrophil membrane phospholipid composition and viability. *Cell Metab.* 21, 51–64. <https://doi.org/10.1016/j.cmet.2014.12.002>.
45. Wang, R., Zhang, T., Chai, Y., Fan, G., Duan, G., Lu, F., and Qi, Y. (2017). Metabolic Disturbances in Inflammatory Bowel Disease and Metabolomics-based Drug Developments Progress. *Pharm. Sci.* 41, 270–277.
46. Peyrin-Biroulet, L., Harmsen, W.S., Tremaine, W.J., Zinsmeister, A.R., Sandborn, W.J., and Loftus, E.V. (2012). Surgery in a population-based cohort of Crohn's disease from Olmsted County, Minnesota (1970–2004). *Am. J. Gastroenterol.* 107, 1693–1701. <https://doi.org/10.1038/ajg.2012.298>.
47. Poggioli, G., Pierangeli, F., Laureti, S., and Ugolini, F. (2002). Review article: indication and type of surgery in Crohn's disease. *Aliment. Pharmacol. Ther.* 16, 59–64.
48. Panes, J., Bouhnik, Y., Reinisch, W., Stoker, J., Taylor, S.A., Baumgart, D.C., Danese, S., Halligan, S., Marincek, B., Matos, C., et al. (2013). Imaging techniques for assessment of inflammatory bowel disease: joint ECCO and ESGAR evidence-based consensus guidelines. *J. Crohns Colitis* 7, 556–585. <https://doi.org/10.1016/j.crohns.2013.02.020>.

49. Bettenworth, D., Bokemeyer, A., Baker, M., Mao, R., Parker, C.E., Nguyen, T., Ma, C., Panés, J., Rimola, J., Fletcher, J.G., et al. (2019). Assessment of Crohn's disease-associated small bowel strictures and fibrosis on cross-sectional imaging: a systematic review. *Gut* 68, 1115–1126. <https://doi.org/10.1136/gutjnl-2018-318081>.
50. Li, X.-H., Mao, R., Huang, S.-Y., Sun, C.-H., Cao, Q.-H., Fang, Z.-N., Zhang, Z.-W., Huang, L., Lin, J.-J., Chen, Y.-J., et al. (2018). Characterization of Degree of Intestinal Fibrosis in Patients with Crohn Disease by Using Magnetization Transfer MR Imaging. *Radiology* 287, 494–503. <https://doi.org/10.1148/radiol.2017171221>.
51. Ordás, I., Rimola, J., Alfaro, I., Rodríguez, S., Castro-Poceiro, J., Ramírez-Morros, A., Gallego, M., Giner, À., Barastegui, R., Fernández-Clotet, A., et al. (2019). Development and Validation of a Simplified Magnetic Resonance Index of Activity for Crohn's Disease. *Gastroenterology* 157, 432–439.e1. <https://doi.org/10.1053/j.gastro.2019.03.051>.
52. Makanyanga, J.C., Pendsé, D., Dikaïos, N., Bloom, S., McCartney, S., Helbren, E., Atkins, E., Cuthbertson, T., Punwani, S., Forbes, A., et al. (2014). Evaluation of Crohn's disease activity: initial validation of a magnetic resonance enterography global score (MEGS) against faecal calprotectin. *Eur. Radiol.* 24, 277–287. <https://doi.org/10.1007/s00330-013-3010-z>.
53. Bourgonje, A.R., Gabriëls, R.Y., de Borst, M.H., Bulthuis, M.L.C., Faber, K.N., van Goor, H., and Dijkstra, G. (2019). Serum Free Thiols Are Superior to Fecal Calprotectin in Reflecting Endoscopic Disease Activity in Inflammatory Bowel Disease. *Antioxidants* 8, 351. <https://doi.org/10.3390/antiox8090351>.
54. Mohammadi, A., Kelly, O.B., Smith, M.I., Kabakchiev, B., and Silverberg, M.S. (2019). Differential miRNA Expression in Ileal and Colonic Tissues Reveals an Altered Immunoregulatory Molecular Profile in Individuals With Crohn's Disease versus Healthy Subjects. *J. Crohns Colitis* 13, 1459–1469. <https://doi.org/10.1093/ecco-jcc/jjz076>.
55. Lunder, A.K., Bakstad, L.T., Jahnsen, J., Borthne, A., Hov, J.R., Vatn, M., and Negård, A. (2019). Assessment of Bowel Inflammation and Strictures by Magnetic Resonance Enterography in Long-term Crohn's Disease. *J. Crohns Colitis* 13, 607–614. <https://doi.org/10.1093/ecco-jcc/jjy208>.
56. Makanyanga, J.C., and Taylor, S.A. (2013). Current and future role of MR enterography in the management of Crohn disease. *AJR Am. J. Roentgenol.* 201, 56–64. <https://doi.org/10.2214/AJR.12.10406>.
57. Bruining, D.H., Zimmermann, E.M., Loftus, E.V., Sandborn, W.J., Sauer, C.G., and Strong, S.A.; Society of Abdominal Radiology Crohn's Disease-Focused Panel (2018). Consensus Recommendations for Evaluation, Interpretation, and Utilization of Computed Tomography and Magnetic Resonance Enterography in Patients With Small Bowel Crohn's Disease. *Radiology* 286, 776–799. <https://doi.org/10.1148/radiol.2018171737>.

STAR★METHODS

KEY RESOURCES TABLE

REAGENT or RESOURCE	SOURCE	IDENTIFIER
Deposited data		
Raw and analyzed data	This paper	N/A
Software and algorithms		
R	Version 4.3.1	https://www.r-project.org/
Vegan	Version 2.6	https://github.com/vegandevs/vegan
ClusterProfiler	Version 4.15.1	https://bioconductor.org/packages/release/bioc/html/clusterProfiler.html
Microeco	Version 1.12.0	https://github.com/ChiLiubio/microeco
Pheatmap	Version 1.0.12	https://doi.org/10.32614/CRAN.package.pheatmap
Ggplot2	Version 3.5.1	https://github.com/tidyverse/ggplot2
Glmnet	Version 4.1–7	https://glmnet.stanford.edu
Python	Version 3.11.3	https://www.python.org/
Scikit-learn	Version 1.3.0	https://scikit-learn.org/stable/
Mediation	Version 4.5.0	https://imai.princeton.edu/projects/mechanisms.html
Origin	Origin2024	https://www.originlab.com
QIIME2 2019.4	N/A	https://docs.qiime2.org/2019.4/tutorials/
Cutadapt	Version 1.2.1	https://github.com/marcelm/cutadapt/
Map2slim	N/A	https://www.metacpan.org
Kraken2	N/A	https://ccb.jhu.edu/software/kraken2/
MMseqs2	N/A	https://github.com/soedinglab/MMseqs2
Megahit	Version 1.1.2	https://github.com/voutcn/megahit
KOBAS	N/A	http://bioinfo.org/kobas/
EggNOG	N/A	http://eggnogdb.embl.de/
CAZy	N/A	http://www.cazy.org/
Chemicals, peptides, and recombinant proteins		
MagBeads FastDNA Kit for Soil	116564384	MP Biomedicals, CA, USA
Other		
NanoDrop NC2000 spectrophotometer	N/A	Thermo Fisher Scientific, Waltham, MA, USA
Vazyme VAHTS DNA Clean Beads	N/A	Vazyme, Nanjing, China
Quant-iT PicoGreen dsDNA Assay Kit	N/A	Invitrogen, Carlsbad, CA, USA
Illumina NovaSeq 6000	N/A	Illumina
Qubit™ 4 Fluorometer	N/A	Invitrogen, USA
TruSeq Nano DNA High Throughput Library Prep Kit (96 samples)	20015965	Illumina, USA
N-(3-(dimethylamino)propyl)-N'-ethylcarbodiimide (EDC)·HCl	N/A	Sigma–Aldrich, St. Louis, MO, USA
Ultraperformance liquid chromatography coupled to tandem mass spectrometry (UPLC–MS/MS)	N/A	ACQUITY UPLC Xevo TQ-S, Waters Corp., Milford, MA, USA
Targeted Metabolome Batch Quantification (TMBQ)	Version 1.0	Metabo-Profile, Shanghai, China
iMAP platform	Version 1.0	Metabo-Profile, Shanghai, China

EXPERIMENTAL MODEL AND STUDY PARTICIPANT DETAILS

Ethics statement

This prospective observational study was approved by Institutional Ethics Review Board of First Affiliated Hospital of Sun Yat-Sen University (No. [2021]215-2). Informed consent was obtained from all participants.

Patient recruitment and specimen collection

From May 2021 to April 2023, 438 patients were consecutively recruited according to the following inclusion criteria: a) patients diagnosed with CD; and b) patients who simultaneously underwent MRE and ileocolonoscopy and provided faecal/serum samples within one week of MRE scanning. The exclusion criteria were as follows: a) antibiotic, probiotic, or prebiotic use three months before inclusion; or b) other concomitant digestive diseases. Thirteen potential participants were excluded because they had antibiotic, probiotic, or prebiotic use in the three months before inclusion (n=11) or other concomitant digestive diseases (n=2) (Figure S1). Therefore, the final patient cohort included 425 subjects.

To illustrate the differences in microecology between HCs and CD patients with different levels of inflammation, we included an additional 42 HCs. HCs were recruited based on matching the age range and sex ratio of CD patients, with their faecal/serum samples collected. Exclusion criteria included gastrointestinal symptoms or the use of antibiotics, probiotics, or prebiotic drugs within three months before enrolment. The faeces were immediately frozen at -80°C . Blood samples were sent directly to the laboratory to obtain serum and frozen at -80°C (Method S2).

The 467 participants were divided into two cohorts: a derivation cohort (CD, n=230; HCs, n=30) and a test cohort (CD, n=195; HCs, n=12) (Table 1). All analyses were derived from the derivation cohort, whereas the test cohort was solely utilized to verify the models' generalizability.

METHOD DETAILS

Grading intestinal inflammation via MRE and ileocolonoscopy

CD patients underwent ileocolonoscopy followed by MRE (Method S3). MRE (including T2-weighted imaging, diffusion-weighted imaging, and pre/postenhancement T1-weighted imaging) was performed using a 3.0T MR system⁵⁰ (protocol detailed in Table S1).

The simplified Magnetic resonance index of activity (sMaRIA)⁵¹ and MR enterography global score (MEGS)⁵² (Table S2) were used to assess transmural inflammation by three radiologists who were blinded to the patients' clinical information. The former encompasses evaluation from the ileum to the rectum, while the latter complements sMaRIA by assessing segments from the jejunum to the rectum, thereby addressing previously unassessed intestinal regions. The simplified endoscopic activity score for Crohn's disease (SES-CD) was employed to quantify mucosal inflammation from the terminal ileum to the colorectum by two gastroenterologists without knowledge of MRE (Method S4). The cut-off values between BI0 and BI1s were SES-CD ≥ 11 ,^{53,54} MEGS score ≥ 10 (small bowel) or MEGS score ≥ 12 (colon),^{55,56} and sMaRIA ≥ 2 .⁵¹ BI1 was defined when at least two of the above criteria were met. Finally, 203 patients were diagnosed with BI0, and 222 exhibited BI1.

Assessment of intestinal inflammation-associated morphological alterations on MRE

The MRE findings of the most severely diseased intestines were jointly evaluated by three radiologists who were blinded to the patients' clinical information.⁵⁷ The imaging features included bowel stricture, penetrating disease, perienteric effusion, comb sign, wall thickness, apparent diffusion coefficient (ADC), T2WI-SI, mural hyperenhancement, mural enhancement pattern, length of diseased bowel, adenopathy, and perianal diseases (Table 2).

Faecal and blood metabolomics

Blood samples were collected from all 467 participants for targeted metabolomics profiling. A total of 245 patients (derivation cohort, n=152; test cohort, n=93) and all 42 HCs provided faecal samples for targeted metabolomics profiling. After Z-transformation of the metabolomic data, partial least squares discriminant analysis (PLS-DA) was conducted to identify differentially abundant metabolites between the groups. Ultimately, 233 faecal metabolites and 529 blood metabolites were identified. Metabolomic experiments, data analyses, and statistical methods are detailed in Methods S1 and S5.

16S rRNA gene amplicon sequencing

16S rRNA gene amplicon sequencing was conducted on all the faecal samples. The alpha diversity was measured with the Chao1, Shannon, and Simpson indices. Mann–Whitney *U* tests were performed to compare alpha diversity. Bray–Curtis distances were calculated, and beta diversity was evaluated. Permutational multivariate analysis of variance (PERMANOVA) was performed with the *adonis* function in *Vegan* (v.2.6) to assess the microbial variance explained by different groups (<https://view.qiime2.org/>). Linear discriminant analysis effect size (LEfSe) was performed to identify the differentially abundant gut microbiota (Methods S1 and S6).

QUANTIFICATION AND STATISTICAL ANALYSIS

The continuous variables were compared between groups via Student's *t* tests or Mann–Whitney *U* tests, whereas chi-square tests were employed to compare discrete variables. Additional statistical methods are described in the corresponding sections of the main text or detailed in Method S1. Benjamini–Hochberg corrections were performed if multiple testing was performed, and the false discovery rate (FDR) was calculated. Statistical analyses were conducted via R statistical software. A significance level of $P < 0.05$ or FDR < 0.05 for multiple testing was applied for all the statistical tests.